CHEMISTRY OF MATERIALS

pubs.acs.org/cm

Article

Quantitative Correlation between Bound Water and Mechanical Stress Relaxation in Dehydrated Metal-Coordinate Polymer Networks

Sungjin Kim,* Myungwoon Lee, Mei Hong, and Niels Holten-Andersen*

Cite This: https://doi.org/10.1021/acs.chemmater.2c01795

Read Online

ACCESS | Metrics & More | Article Recommendations | Supporting Information

ABSTRACT: Dynamic metal-coordinate cross-links impart smart and superior physicochemical properties in their deployments in many biological and artificial metallopolymer networks in various stages of solidification via dehydration. Nonetheless, a quantitative model that describes to what extent the dynamic behaviors of metal-coordinate bond transition from the hydrated to the dehydrated state is missing. In previous work, we have shown that local water binding helps metal-coordinate bonds to maintain their dynamic properties during bulk network dehydration, thereby offering mechanical damping properties to the network deep into the dehydrated solid state. Using mussel-inspired hydrogels with chemically tuned fractions of metal-coordinate cross-links, here, we reveal the direct scaling relationship between the macroscopic relaxation time of the dehydrated network and the amount of microscopic water bound by metal-coordinate cross-links. This quantitative relationship between dehydrated metal-coordinate network mechanics and metal-coordinate cross-link dynamics may help us better understand and emulate the sustainable process of solidification via spatiotemporally controlled dehydration of load-bearing materials on wide display in nature.

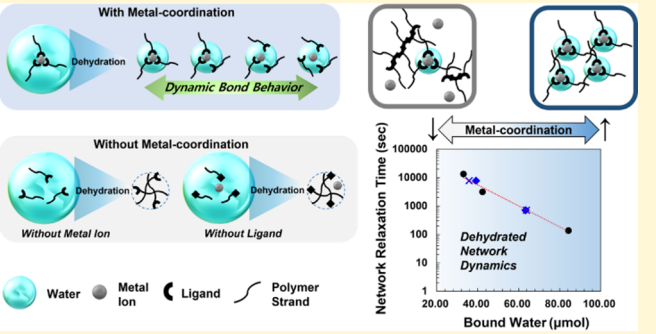

Many biological macromolecular organic−inorganic materials exhibit inspiring mechanochemical properties, thanks to the strong, reversible bonds present in dynamic supramolecular assemblies such as metal-coordinate bonds.[1−9] Found in various marine biological materials including marine worm jaws[6,10−13] and mussel holdfast fibers,[1,5,14−25] metal-coordinate cross-links possess unique properties responsible for the mechanochemical behaviors displayed by these materials: (i) metal-coordinate bond strength can approach that of covalent bonds (based on single-molecule force spectroscopy measurements[24]); (ii) metal-coordinate bonds are kinetically labile; thus, they can dynamically break and reform to dissipate energy and recover structural damage from external shocks; and[4,26,27] (iii) metal-coordinate cross-linking can be triggered by external stimuli such as pH changes, offering material stimuli-responsiveness.[2,6] Mussels, in particular, take advantage of several of these traits of metal-coordinate cross-linking in the robust tethering holdfast of their byssal threads.[15] Each of these proteinaceous holdfast fibers is composed of an inner core and an outer cuticle. The collagen proteins in the core are partially cross-linked via histidine side groups coordinating with ions of transition metals like Cu and Zn,[16,17] while the catecholic proteins of the cuticle are partially cross-linked by coordination complexes with ions of transition metals including Fe and V (Figure 1).[18−21] Substantial evidence suggests that the metal-coordinate cross-links in mussel byssal threads and their biomimetic derivatives enable enhanced mechanical energy dissipation during dynamic loading in hydrated conditions.[16−21] However, mussel byssal threads experience dramatic changes in hydration levels in their natural intertidal habitat,[28−30] and our understanding of the extent to which metal-coordinate cross-links retain their dynamic behavior during bulk material solidification via dehydration is very limited.[31] More generally, elucidating the role of water in controlling any dynamic bond behaviors in aqueous networks transitioning from fully solvated swollen states to desolvated condensed states may lead to a universal understanding of the critical steps during solidification via dehydration of both natural and synthetic macromolecular networks highly relevant for new sustainable material processing strategies.

In a previous study of the dehydration effects on mussel-inspired metal-coordinate hydrogels, evidence suggested that Fe−catechol coordinate bonds retain their mechanical energy-dissipative properties after gel dehydration through local water

Received: June 16, 2022
Revised: November 2, 2022
Published: November 30, 2022

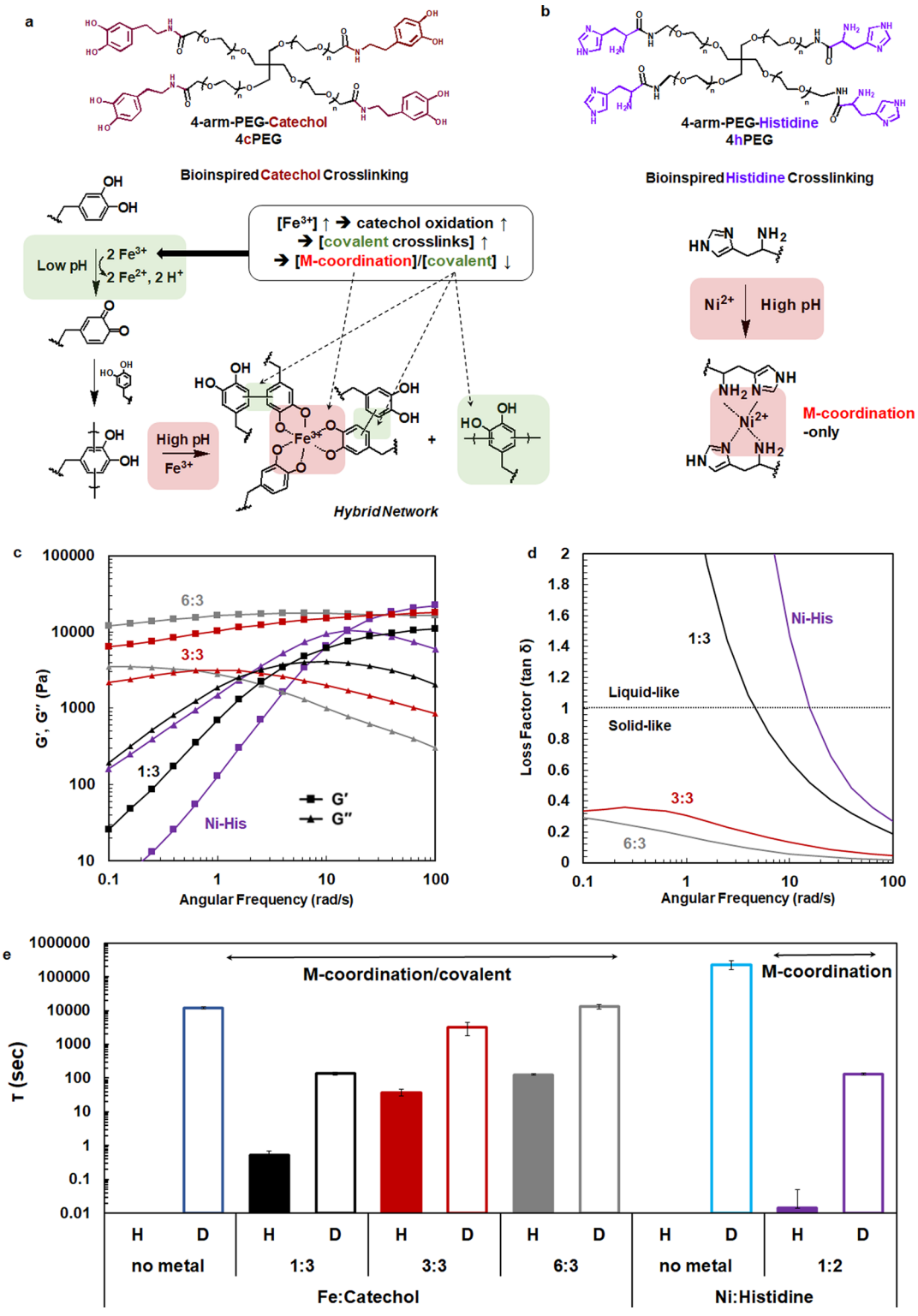

Figure 1. (a) Bioinspired catechol cross-linking path to form a hybrid gel network cross-linked by both dynamic metal-coordinate bonds and permanent covalent bonds. Fe^{3+} are known to initially oxidize catechols to induce covalent cross-linking; thus, increased [Fe^{3+}] indicates the higher fractions of covalent bonds within the network. (b) Compared histidine cross-linking path where only the metal-coordinate cross-linking takes place for network formation. Note that the depictions in both (a) and (b) are conceptual and not meant to describe the detailed chemical structure of the final network. (c) Viscoelastic response of hydrogels formed with different [Fe]/[catechol] ratios (1:3, black; 3:3, red; 6:3, gray) and [Ni]/[histidine] of 1:2 as a covalent-free counterpart (purple) at pH 10 to oscillatory shear at 1% strain at 25 °C. (d) Loss factor (tan $\delta = G''/G'$) of the same data in (c). (e) Comparison of relaxation times (τ) for hydrated (H) and dehydrated (D) samples of each condition. The metal-free systems of catechol and histidine polymer networks were used as controls without cross-links. τ was obtained by fitting Kohlrausch's stretched−exponential relaxation model (eq 1) to stress-relaxation curves shown in Figure S1.

https://doi.org/10.1021/acs.chemmater.2c01795
Chem. Mater. XXXX, XXX, XXX−XXX

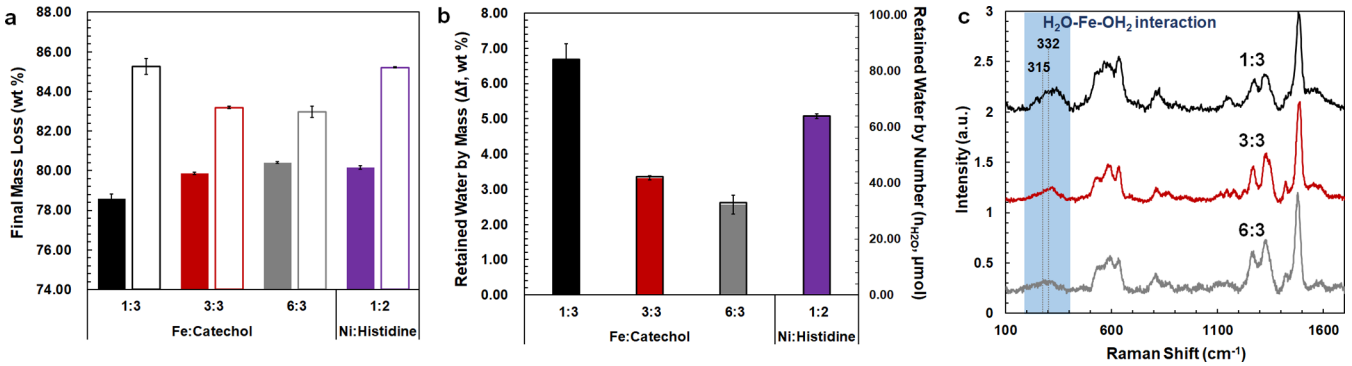

Figure 2. (a) Water loss (wt %, eq 4 in the Experimental Methods section) of each sample from TGA measurements (Figure S2). The coordination-present samples (colored bars, left) exhibit lower water mass loss than the coordination-absent samples (blank bars, right). (b) Amount of water retained after dehydration by its weight fraction (left axis) and the number of water molecules (right axis). The retained water fraction (Δf, wt %, colored bars, left y-axis) was calculated by subtracting the final water loss of the coordination-present sample from that of the coordination-absent counterpart (eq 5 in the Experimental Methods section). The number of H_2O bound by metal coordination (n_{H_2O}, μmol, outlined bars, right y-axis) was derived by multiplying the above Δf by the original mass of the hydrogel divided by the molecular weight of water (eq 6 in the Experimental Methods section). The temperature was increased from 23 to 140 °C with a rate of 5 °C/min (i.e., total 23.4 min ramp time) in air. (c) Raman spectra of the systems with Fe/catechol ratios of 1:3, 3:3, and 6:3 dehydrated at 20 °C over 48 h in 16% R.H. The spectra have been normalized in reference to the strongest peak at 1480 cm^{-1}. Detailed peak assignments are listed in Table S1.

binding.[32] Nevertheless, the quantitative correlations between the dehydrated network dynamics, the density of metal-coordinate cross-links, and the amount of bound water in the network were not elucidated. Moreover, other than studies of Fe−catechol bonding, little work has been done to investigate whether metal−ligand complexation more broadly displays water binding capabilities. Therefore, here we attempted to elucidate the quantitative relationship between the evolving time scale of network stress-relaxation and the amount of water retained by two different metal-coordinate cross-links during network dehydration: Fe−catechol and Ni−histidine coordination complexes. We found that the stress-relaxation time scale and the amount of bound water of dehydrated networks were both determined by the concentration of metal-coordinate complexes via a quantitative relationship that follows a negative-exponential scaling. These new findings help us advance our understanding of the role of the water-binding capability of metal-coordinate bonds in controlling the viscoelastic properties of macromolecular networks undergoing solidification via dehydration, knowledge which could turn out to be critical to the future success of sustainable material processing platforms.

We used four-arm PEG modified with either catechol (4cPEG) or histidine (4hPEG) to form polymer hydrogels cross-linked via metal coordination with Fe^{3+} or Ni^{2+}, respectively, as the platforms for our study. In the Fe−catechol system, we can control the amount of metal-coordinate cross-links relative to permanent covalent cross-links within the network by simply adjusting the Fe^{3+} concentration (Figure 1a). On the other hand, the Ni−histidine system contains only metal-coordinate cross-links, thus behaving as a purely transient network (Figure 1b).[33,34] In the Fe−catechol networks, it is known that Fe^{3+} ions form *tris*-Fe−catechol coordination complexes at basic pH (>8.5), while the excess Fe^{3+} ions are also known to oxidize catechols to induce covalent dicatechol cross-linking under the initially acidic pH before the pH jump for Fe coordination.[35,36] Thus, by adjusting the concentration of Fe^{3+} mixed with 4cPEG (e.g., [Fe]/[catechol] = 1:3, 3:3, 6:3), we can control the fractions of permanent covalent and dynamic metal-coordinate cross-links in the resulting covalent/metal-coordinate hybrid networks (Figure 1a). To our satisfaction, the hydrogel formed with the 1:3 mixing ratio, assumed to stoichiometrically form cross-links of mostly *tris*-Fe−catechol coordination, exhibited the most fluidlike behavior. The 1:3 hydrogel showed the fastest network relaxation demonstrated by the dynamic oscillation frequency of ∼5 rad/s at which fluidlike behaviors (represented by loss modulus G'') take over solidlike behaviors (represented by storage modulus G') of the network (Figure 1c). In contrast, the hydrogels formed with 3:3 and 6:3 mixing ratios show increasingly solidlike behavior as shown by the $G' > G''$ and less frequency-dependent G' trends in the measured frequency region. The control over the network dynamics by the Fe−catechol cross-linking chemistry can be further supported by the loss factor ($\tan\delta = G''/G'$) (Figure 1d). The liquidlike, energy-dissipative behavior shown by the high $\tan\delta$ of the 1:3 network is in sharp contrast with the low $\tan\delta$ of the 3:3 and 6:3 hydrogels, indicating the solidlike, energy-storing behavior. Consistent with these comparisons, the *bis*-Ni−histidine-coordinate cross-linked hydrogels with only metal-coordinate cross-links show even faster relaxation (Figure 1c) and a higher loss factor (Figure 1d) than 1:3 hydrogels at the same tested pH 10. These observations confirm the dynamic nature of metal-coordinate cross-links in contrast to the permanent covalent cross-links and tunable viscoelasticity of the hydrogels, as demonstrated previously by Barret et al.[36] Thus, these metal-coordinate networks serve as a good controllable platform for testing the dehydration effects on the dynamic behaviors transitioned from their wet hydrogel state to the dehydrated xerogel state.

To examine whether the dynamic nature of the metal-coordinate cross-links persists upon dehydration, we characterized the changes in viscoelastic properties upon dehydration (Figures 1e and S1). To evaluate the macroscopic dynamic behavior of the network quantitatively, we analyzed the relaxation time (τ) (Figure 1e) from the stress-relaxation profiles of hydrated (Figure S1a,e, denoted H) and dehydrated gels (Figure S1d,h, denoted D). As the relaxation curves of many viscoelastic polymer materials follow Kohlrausch's

https://doi.org/10.1021/acs.chemmater.2c01795
Chem. Mater. XXXX, XXX, XXX−XXX

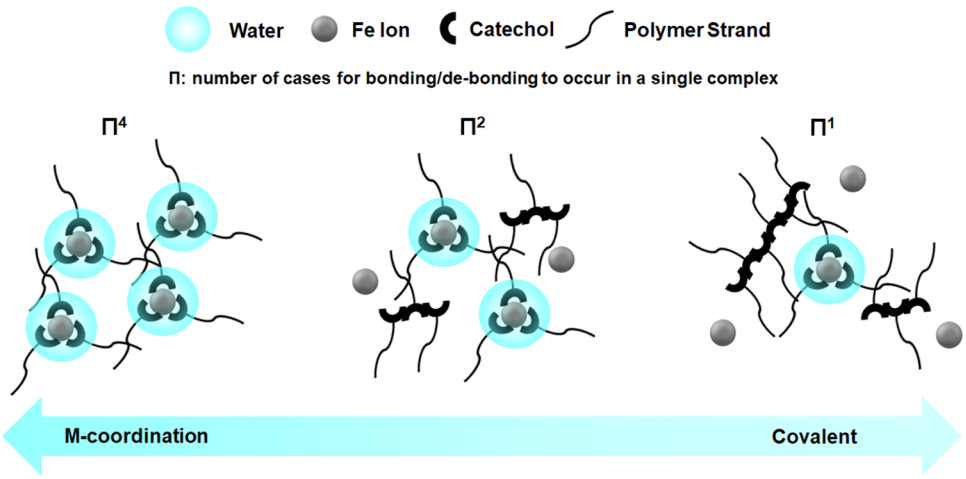

Figure 3. Proposed schematics on the dynamic behavior of the dehydrated Fe−catechol networks of the different ratios between the metal-coordinate bonds to covalent bonds within the cross-linked network. Given that a single metal-coordinate complex binds water molecules to form multiple hydration layers, the metal-coordination-dominant network contains more metal-coordinate complexes with hydration shells within the system. We infer that these hydration shells serve as a local medium facilitating the metal-coordinate complex to exhibit their dynamic bonding and debonding activities. Thus, the dynamic behavior of a network will become prominent as the total number of the complex with hydration shells ($n_{complex}$) in the system increases. Then, the total number of cases that coordination center metals bond or debond with ligands in a network (Πtot) can be quantified by multiplying all ($n_{complex}$) individual sets of the number of cases for dynamic bonding activities in each complex (Π_i) as $\Pi_1 \times \Pi_2 \times \cdots \times \Pi_{n_{complex}} = \Pi^{n_{complex}}$ where $\forall i$, $1 < \Pi_i = \Pi$ for the same type of metal−ligand complex. For instance, if there is only one complex in a network, $\Pi tot = \Pi^1$ (right); if there are two, $\Pi tot = \Pi^2$ (middle); if four, $\Pi tot = \Pi^4$ (left). Therefore, the dynamic bonding activities within a defined timeframe (i.e., the rate of the dynamic behaviors) in the network would be proportional to Πtot. This concept model can explain the dynamic behavior associated with water retention in a dehydrated network where metal-coordinate bonds are present.

stretched−exponential relaxation model, the τ could be derived by eq 1

$$G(t) = G_0 \exp\left[-\frac{t}{\tau}\right]^{\alpha}, \quad 0 < \alpha < 1 \tag{1}$$

where G_0 is a plateau modulus, α is the fitting parameter dictated by the physical constraints of each system, and τ is the characteristic relaxation time.[37−39] Surprisingly, the τ values of not only the hydrated but also the dehydrated states of networks were shorter (i.e., more dynamic) as the metal-coordinate cross-links become dominant in the network (i.e., $\tau(1{:}3) < \tau(3{:}3) < \tau(6{:}3)$). This confirms that the 1:3 system is indeed the most dynamic Fe−catechol network in the dehydrated state (Figure S1d) as well as in the wet state (Figure S1a). The Ni−histidine network with only metal-coordinate bonds also showed shorter τ values in both hydrated and dehydrated states than all other networks containing covalent bonds. Importantly, the relaxation times of both coordination-dominant networks (i.e., 1:3, Ni−His) after dehydration are around 100 and 1000 times shorter than those of their corresponding metal-free (blank) counterparts with no cross-links. These results corroborate that the metal-coordinate bonds after dehydration ended up more dynamic than any other inter-/intramolecular interactions between the uncross-linked polymer strands under dehydration-induced solidification.

To investigate the relationship between the network-bound water and the metal-coordinate cross-links, we sought to directly compare the water loss and the water loss rate with or without the presence of metal-coordinate bonds in the polymer networks. We, therefore, conducted thermogravimetric analysis (TGA) on the metal-coordinating catechol (Figures 2 and S2a−c) and histidine (Figures 2 and S2d) systems in comparison with ligand-free control systems with otherwise identical compositions. Note that the coordination-free PEG systems did not retain water after dehydration by ambient drying or thermal increment in TGA.[32] All coordination-present systems clearly showed less and slower water loss than the coordination-absent systems (Figures 2a and S2a−d). Especially, the Fe−catechol coordination-present systems displayed a trend of less water loss with lower [Fe^{3+}] (Figure 2a). In addition, all of the coordination-present systems exhibited a similar maximum mass loss rate (∼1.8%/°C) and kept losing mass until ∼110 °C to reach their equilibrium (Figure S3). These results are interesting since they appear to contradict a common notion of colligative properties. Typically, more solutes present in a hydrogel should decrease its relative water loss (i.e., $(m_i - m_d)/m_i$, where m_i and m_d indicate the initial wet mass and dry mass, respectively) due to the mass conservation of nonvolatile solute particles (i.e., higher m_d) and slow down the water loss rate by suppressing vaporization at the water−air interface (i.e., Raoult's law). This common view indeed applies well to the coordination-absent systems, which behaved like a classic general solution where the sample with the least amount of solutes (i.e., 1:3) showed the greatest water loss (Figure 2a), the fastest water loss rate (∼2.4%/°C), and the lowest equilibrium temperature (∼90 °C) (Figure S4). Like Fe−catechol coordination-present system, the decrease in the mass loss rate against temperature increment was also found in the Ni−histidine coordination-present system (Figures S2d and S5). These observations thereby support our hypothesis that the amount of bound water in the coordination-present networks is predominantly controlled by the fraction of metal-coordinate cross-links, overwhelming the colligative properties.

To quantify the amount of water conserved by metal coordination against dehydration, we derived the number of water molecules (n_{H_2O}) from the difference in the water loss

https://doi.org/10.1021/acs.chemmater.2c01795
Chem. Mater. XXXX, XXX, XXX−XXX

between the coordination-absent and coordination-present systems (Δf) (Figure 2b, eqs 4−6 in the Experimental Methods section). The ascending order of water retention (Δf, n_{H_2O}) among the Fe−catechol systems is consistent with the ascending order of the fraction of metal-coordinate cross-links. The retained water in Fe−catechol coordination systems could be also evidenced by Raman spectroscopy (Figure 2c), where all samples exhibited the characteristic vibration bands reported previously for Fe−catechol coordinations (Table S1).[2,37] Here, the band at ∼320 cm^{-1} attributed to the Fe−H_2O interactions[32,40−42] showed the different intensities among the three samples: strong for 1:3, medium for 3:3, and weak for 6:3. This trend agrees well with the comparative water retention calculated in Figure 2b. Note that the noncoordinated Fe^{3+} did not have a distinguishable influence on this signal.[32] Moreover, ^1H NMR spectroscopy proved the existence of mobile H_2O molecules responsive to the magnetic field[43−46] in the 1:3 system (Figure S6) with the most retained water (Figure 2b). These spectroscopic results further support the water retention trends we observed using mass measurements (Figures 2a,b, S2, and S3).

Based on these results, we tried to establish a base mechanism model to quantitatively address the correlation between the metal-coordinate cross-links and the water retention of the networks after dehydration (Figures 1 and 2). We observed that the metal-coordination-rich network stays dynamic and binds water in contrast to the metal-coordination-free uncross-linked counterpart that retains little water and hardly behaves dynamically after dehydration (Figures 1e and 2).[32] Hence, it is reasonable to consider that the network-bound water remains close to the metal-coordinate cross-linking sites rather than elsewhere in the polymer backbone. Thus, while we note that the metal-coordinate bonds can still be dynamic without observed water,[3,47,48] we infer this locally "wet" condition of metal-cross-linking sites can facilitate the dynamic behaviors beyond those expected in the perfectly water-deplete state (Figure S7) since the dynamic exchange of metal-coordinate cross-links can be assisted by solvents.[49] Therefore, we postulated that a defined number of water molecules are bound to each metal-coordinate complex keeping the metal-coordinate bonds locally wet and facilitating their dynamic behavior after dehydration (Figure 3, Figures S7). We previously viewed that each metal-coordinate complex is surrounded by multiple hydration layers like other water-binding macromolecules.[32,50,51] Our calculated number of bound water molecules (Figure 2b) is consistent with such interpretations. Using the 1:3 Fe−catechol system as a reference, we regarded that every Fe^{3+} (0.3 μmol) here forms a tris-coordination complex with catechols (0.3 μmol). Then, 84.26 μmol retained H_2O molecules (n_{H_2O}, Figure 2b) here must be bound to the coordination complexes, forming multiple hydration layers since a single coordination complex cannot accommodate 280 water molecules within the first octahedral coordination shell (i.e., the binding capacity of 8 water molecules). This rationale for the existence of multiple hydration layers surrounding the coordination complex applies also to our other systems (Table S2 for details). We propose that these hydration shells function as the local medium, wherein the coordination bonds can be facilitated to be mobile enough after dehydration to bond and debond possibly through dynamic exchange between the metals or ligands and surrounding water molecules, as seen from our stress-relaxation data (Figure S1). We infer that these water molecules can exchange bonding between the catechols and metals within the first hydration layer. The coordination-absent systems, without either metal ions or ligands, do not provide these hydration shells after dehydration.[32] Thereby, the dehydrated coordination-free polymer chains face the physical penalties for their movement and exhibit a behavior close to a covalent-dominant network, even though they are not chemically cross-linked (Figures 1e, S1d,h, and S8).

To rationalize our hypothesis that the water is bound to each metal-coordinate complex to maintain the metal-coordinate bond dynamics, we attempted to find a direct quantitative correlation between the number of retained water molecules and the dynamic behavior of dehydrated metal-coordinate networks. Our suggested water-binding metal-coordinate cross-link dynamics can be demonstrated through the following rationales: (i) as we proposed, the metal ion can still bond and debond with different ligands with equal probabilities within a coordination complex that forms hydration shells persisting after dehydration. (ii) Coordination complexes of the same type of metal−ligand pair have equal capabilities of binding water to form hydration layers, possibly via the metal ion coordinating partly with water molecules within the coordination sphere (Figure S7).[32,40−42] In other words, n_{H_2O} is proportional to the number of coordination complexes (i.e., $n_{complex} \propto n_{H_2O}$, $n_{complex} < n_{H_2O}$) and n_{H_2O} bound per complex ($\underline{n_{H_2O}} = n_{H_2O}/n_{complex}$) stays constant for the same type of metal−ligand coordination complex (e.g.,$\underline{n_{H_2O}}$ values of Fe−catechol complexes are the same in all 1:3, 3:3, and 6:3 systems, see Table S2 for details). (iii) The rate of dynamic behaviors of the network is inversely proportional to the network relaxation time τ. We use the relaxation frequency (i.e., reciprocal relaxation time, $\upsilon = 1/\tau$) as the indicator of the dynamic behavior rates. (iv) Finally, this υ will be increased by the increase in the total number of cases (Πtot) of different coordination centers (i.e., coordinating metal ions) interacting with available ligands in the network. Here, we define the possible number of cases that one coordination center bonds or de-bonds the ligands within a single individual complex as Π_i ($\Pi_i > 1$, the value is specific to the type of metal−ligand complex and is not meant to determine the actual number of cases of microscopic metal−ligand bonding activities). Now, we can deduce that υ and Πtot should exponentially increase as the number of coordination complexes surrounded by hydration shells increases as follows (Figure 3)

$$\upsilon = \frac{1}{\tau} \propto \Pi\text{tot} = \prod_{i=1}^{n_{complex}} \Pi_i = \Pi^{n_{complex}} = \pi^{n_{H_2O}}$$
$$\text{or } \tau \propto \pi^{-n_{H_2O}} \quad (2)$$

where for all i's, $\Pi_i = \Pi > \pi > 1$ for the same type of metal−ligand complex. If our suggested model is valid, our experimental data of τ (Figure 1e) and n_{H_2O} (Figure 2b) should follow the quantitative relation from eq 2 as follows

$$\frac{\upsilon_b}{\upsilon_a} = \frac{\tau_a}{\tau_b} = \pi^{n_{H_2O}(b) - n_{H_2O}(a)} \quad (3)$$

where subscripts a and b denote two different individual systems containing the same type of coordination complexes, respectively. As displayed in Figure 4, this model fits our obtained data of Fe−catechol systems with an R^2 of 98.02%

https://doi.org/10.1021/acs.chemmater.2c01795
Chem. Mater. XXXX, XXX, XXX−XXX

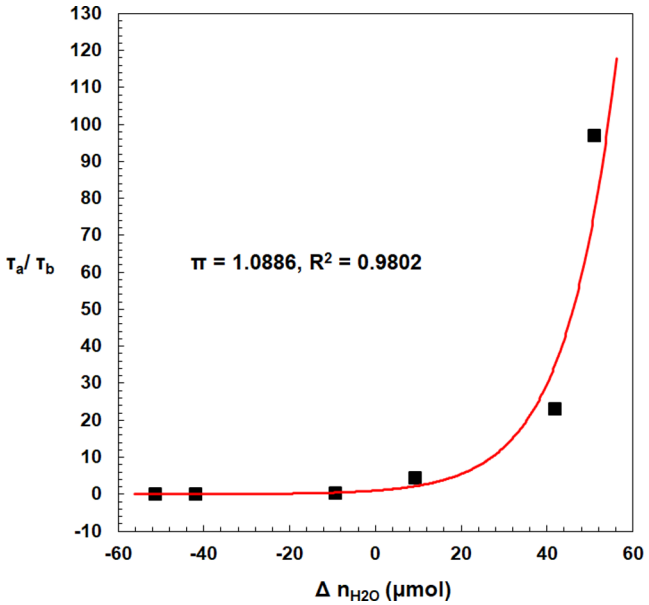

Figure 4. Plots displaying Δn_{H_2O} (n_{H_2O}(b)−n_{H_2O}(a)) vs τ_a/τ_b from our experimentally obtained data of τ by eq 1 from Figure 1e and n_{H_2O} from Figure 2b (black square dots) of the Fe−catechol system and the electronically fitted curve (red). Subscripts a and b indicate two different systems: system a and system b. The fitted plot shows the direct exponential relation (eq 3) between the two parameters (Δn_{H_2O}, τ_a/τ_b) with an R^2 of 98.02%. More information on the fitting process is available in Tables S3 and S4 and Figure S9.

(more details are in Tables S3, S4, and Figure S9). In addition, we further obtained τ from additional step-strain tests on [Fe]/[catechol] = 2:3 and 4:3 (i.e., n_{H_2O} of 1:3 > 2:3 > 3:3 > 4:3 > 6:3 from the trend in Figure 2) and found they also abide by our established model (Figure S10). These results thereby support that the number of retained water molecules, without other variables, directly correlates with the dynamic behavior represented by τ of dehydrated networks containing metal-coordinate cross-links.

Using this model, we can estimate the relaxation time and the amount of bound water of a dehydrated network containing Fe−catechol cross-links by specifying either parameter. Although a detailed single molecular/atomic level of bonding activity within a coordination complex is yet to be clarified, we note that our model resembles an Arrhenius-type equation at a constant temperature that describes a general rate of bond association/dissociation, which hints at future investigation toward a better understanding of the dynamic bond mechanism in a dehydrated network. In addition, it is known that hydrogen bonds can exist between water and both catechols and Fe^{3+},[52,53] thus it is tempting to speculate that hydrogen bonding may contribute to water binding and water exchange between the catechols and Fe^{3+}, which help dynamic behaviors of the metal-coordinate bonds. Our findings may suggest a candidate explanation for dehydration-mediated biomechanical properties in biological materials, for example, the steadfast, hyperextensible mussel byssus thread cuticles containing soft microgranules rich in Fe−catechol coordination, preserving hydration upon exposure between tidal cycles.[31] More broadly, our model may be applied to predict and tailor the hydration-related physicochemical, biochemical, and electrochemical properties of metal-coordinate materials including metal-catecholic or -phenolic networks for applications ranging from catalysis, controlled release, and tissue engineering to dyes and displays.[54−57] Furthermore, the dynamic bond behaviors transferred from a soft, wet state to a hard condensed state may have important implications in material processing and manufacturing technologies involving solvent-evaporative fluid-to-solid transition such as adhesion, mold casting, or additive manufacturing.[58,59]

We have presented a quantitative model that rationalizes metal-coordinate bonds staying dynamic upon dehydration, assisted by their water-retaining capability, which controls the dehydrated network dynamics. By chemically controlling the metal-coordinate cross-linking, we have demonstrated the tunability of both the relaxation time and bound water of the network after dehydration. Based on these observations, we found the scaling relationship between the stress-relaxation time and the water retention of dehydrated metal-coordinate networks. This model allows us to quantitatively predict the mechanochemical properties of dehydrated, seemingly dry metal-coordinate networks by inspecting their remnant water content and vice versa. Our findings together imply that simply tuning the metal coordination in the aqueous state can program the spatiotemporal mechanical behavior of the dehydrated metallopolymer network, for instance, to be 100 times more dynamic than the uncross-linked polymer in the dehydrated solid state. The dehydrated metal-coordinate bond dynamics investigated here, therefore, may offer insights into smarter utilization of metal-coordinate bonds toward sustainable material processing strategies inspired by biological metallopolymer solidifications widely displayed in nature.

EXPERIMENTAL METHODS

Safety Statements. No unexpected or unusually high safety hazards were encountered during the experimental procedures described below.

Materials. Four-arm-PEG-NHS (4aPEG-NHS, 10 kDa) and 10 kDa 4-arm-PEG-NH_2 (4aPEG-NH_2) were purchased from JenKem Technology USA, Inc. Inorganic salts including iron(III) chloride hexahydrate ($FeCl_3 \cdot 6H_2O$), nickel(II) chloride hexahydrate ($NiCl_2 \cdot 6H_2O$), and sodium hydroxide (NaOH) were purchased from Sigma-Aldrich unless indicated otherwise. All other organic ingredients were purchased from Sigma-Aldrich.

Synthesis of 4cPEG. Four-arm-PEG-catechols (4cPEG) were synthesized following a previously reported process,[32,34] with some modifications: dopamine hydrochloride (dopa-HCl) (1.5× molar relative to −NHS) was mixed with 4aPEG-NHS and dissolved in 10 mL of anhydrous *N*,*N*-dimethylformamide (DMF) in a Schlenk flask. Then, the reaction was initiated by adding triethylamine (TEA) (2.5× molar equivalent relative to −NHS) to substitute −NHS to −catechols. The flask was protected with N_2 gas. The reaction was proceeded in the flask in a 55 °C silicone oil bath for 12 h to produce 4cPEG. After the reaction, the flask was cooled down to room temperature. Then, the organic phase with the product and the aqueous phase with the salts were separated by adding 20 mL of chloroform and 20 mL of water followed by extracting the organic phase from the mixture. Na_2SO_4 was added to the above organic solution to remove any remnant water. The organic solvent was evaporated by a rotary evaporator. Then, the product was purified via precipitating in diethyl ether, followed by redissolving in 5 mL of dichloromethane (DCM). After repeating the above purification steps three times, the precipitate was dried under a vacuum. The final purified product (4cPEG) was obtained by freeze-drying.

Synthesis of 4hPEG. Four-arm-PEG-histidine (4hPEG) was synthesized following the method reported previously.[33] In short, 5.0 g of 4aPEG-NH_2 (10 kDa) was mixed with 1.49 g of Boc-His(Trt)-OH and 1.33 g of BOP reagent in 15 mL of dichloro-

https://doi.org/10.1021/acs.chemmater.2c01795
Chem. Mater. XXXX, XXX, XXX−XXX

methane (DCM) in a Schlenk flask protected with N_2 gas, as described before. About 1.07 mL of *N*,*N*-diisopropylethylamine (DIPEA) was then added to start the reaction and proceeded for 2 h. The product was obtained by precipitating in diethyl ether, followed by purification through dissolving and precipitating in methanol under −20 °C three times, and then precipitating again in diethyl ether. The product was vacuum-dried and then went through the deprotection process for 2 h in the cleavage solution of 95 mL of trifluoroacetic acid (TFA), 2.5 mL of triisopropylsilane, and 2.5 mL of water. The solvent was then removed via rotary evaporation. The product was again purified by redissolving in methanol and precipitating in diethyl ether. The purification step was repeated three times, and the final product (4hPEG) was obtained by lyophilization, as described above for 4cPEG.

Formation of Fe-4cPEG Hydrogels. Fe-4cPEG hydrogels (20 μL) were formed by adding $FeCl_3{\cdot}6H_2O$ to the aqueous 4cPEG (200 mg/mL) solution followed by a pH jump. The hydrogels were formed in the [Fe^{3+}]/[catechol] ratios of 1:3, 3:3, and 6:3; then, the pH was controlled to ∼10 via adding NaOH to form dark red gels. For convenience, we use the [catechol]/[Fe^{3+}] ratio to label the different Fe-4cPEG samples studied. The final polymer concentration in hydrogels was 125 mg/mL for all types of Fe-4cPEG hydrogels. The final concentrations Fe^{3+} were 15 mM for 1:3, 50 mM for 3:3, and 100 mM for 6:3. The final concentrations of NaOH in the hydrogels were 100 mM for 1:3, 200 mM for 3:3, and 304 mM for 6:3.

Formation of Ni-4hPEG Hydrogels. Ni-4hPEG hydrogels (20 μL) were formed by adding $NiCl_2{\cdot}6H_2O$ to the aqueous 4cPEG (200 mg/mL) solution followed by a pH jump. The hydrogel was formed in the [Ni^{2+}]/[histidine] ratio of 1:2; then, the pH was controlled to ∼10 via adding NaOH to form clear gels. The final polymer concentration in hydrogels was 125 mg/mL. The final concentration of Ni^{2+} was 25 mM, and that of NaOH was 125 mM.

Rheological Measurement. The rheometric measurement was performed using an Anton Paar MCR 302 rheometer (Anton Paar). The hydrogels (20 μL) were placed under the 10 mm diameter parallel plate geometry. The measurement was proceeded at 25 °C under a solvent trap for blocking evaporation during the operation. Oscillatory frequency sweeps were performed at a constant 1% strain and angular frequency ranging from 100 to 0.1 rad/s to obtain the storage (G') and loss (G'') moduli and the corresponding loss factor ($\tan\delta = G''/G'$). Stress-relaxation tests were performed under 10% step-strain (γ), and the stress (σ) and relaxation modulus ($G(t) = \sigma/\gamma$) were recorded over a time passage of 1000 s. The samples were dehydrated for 0.25 h (15 min), 2.75 h (2 hr 45 min), 6.75 h (6 hr 45 min), and 17.75 h (17 hr 45 min) at 25 °C and 16% relative humidity (R.H.) and before each test. Note that drying over 17.75 h no longer resulted in a significant difference in water loss.[32]

Thermogravimetric Analysis (TGA). Each sample (20 μL) was analyzed by a TGA Q500 (TA Instruments) to perform dehydration. The temperature was ramped up from 23 to 140 °C at a rate of 5 °C/min in air with a gas flow rate of 60.0 mL/min. The water mass loss (f, i.e., the mass ratio between the lost water and the initial hydrogel) (wt %) was calculated by the following equation

$$\text{mass loss (wt \%)} = f = \frac{m_i - m}{m_i} \times 100 \tag{4}$$

where m_i is the initial mass of the wet hydrogel and m is the mass of the gel recorded during the measurement. Derivative thermogravimetric analysis (DTG) was conducted using TA Analysis 2000 Software (TA instruments) to obtain the rate of mass loss (%) per temperature increase (dm/dT, %/°C). Based on this equation, we calculated the amount of retained water as follows

$$\text{retained water (wt \%)} = \Delta f = f_2 - f_1 \tag{5}$$

where f_1 is the water mass loss (wt %) with metal coordination and f_2 is that without metal coordination (i.e., f of the corresponding system without the metal-coordinating ligand and otherwise identical compositions) when the respective TGA curve plateaus (Figure S2). Thus, we can also compute the total number of H_2O molecules (n_{H_2O}, μmol) bound by metal coordination in a system as follows

$$n_{H_2O}\ (\mu\text{mol}) = \frac{m_i \Delta f}{100} \times \frac{1}{M_{H_2O}} \times 10^6 \tag{6}$$

where m_i (g) is the original mass of each hydrogel before dehydration and M_{H_2O} is the molecular weight of water (18 g/mol).

Raman Spectroscopy. Raman spectroscopy analysis was performed using a Raman spectrometer—LabRAM Raman confocal microscope (HORIBA Jobin Yvon) with a 785 nm near-IR laser excitation. Samples were loaded on a glass substrate, which was placed on a Märzhäuser stage (Märzhäuser Wetzlar). Then, the stage was positioned under a 10× microscope lens. The laser power was 30 mW. The grating was 600 g/mm. The filter was adjusted to 10%. The integration time was 2 s with an accumulation of five times. The samples (20 μL) were dehydrated over 48 h at 20 °C and 16% R.H. before the measurement. Measurements and data collection were performed using LabSpec 6 (Horiba Scientific) software.

Nuclear Magnetic Resonance (NMR) Spectroscopy. Solid-state NMR spectra for the dehydrated gels were measured by a Bruker 400 MHz (9.4 T) spectrometer (Bruker Corp) using 4 mm magic angle spinning (MAS) probes. 1D ^1H direct-polarization (DP) spectra were measured at 298 K under 5 kHz MAS frequency. Each sample (20 μL) was dehydrated over 48 h at 20 °C and 16% R.H. before loading on the probes.

■ ASSOCIATED CONTENT

Supporting Information

The Supporting Information is available free of charge at https://pubs.acs.org/doi/10.1021/acs.chemmater.2c01795.

Additional information on stress-relaxation analyses, TGA, DTG, Raman spectroscopy, solid-state H NMR, rheometry, and quantitative modeling (PDF)

■ AUTHOR INFORMATION

Corresponding Authors

Sungjin Kim − *Department of Materials Science and Engineering, Massachusetts Institute of Technology, Cambridge, Massachusetts 02142, United States;* Present Address: Chemical Sciences Division, Oak Ridge National Laboratory, Oak Ridge, Tennessee 37831, USA; orcid.org/0000-0002-2068-9189; Email: kims1@ornl.gov

Niels Holten-Andersen − *Department of Materials Science and Engineering, Massachusetts Institute of Technology, Cambridge, Massachusetts 02142, United States;* Present Address: Department of Materials Science and Engineering, Department of Bioengineering, Lehigh University, Bethlehem, Pennsylvania 18015, USA; orcid.org/0000-0002-5318-9674; Email: nih221@lehigh.edu

Authors

Myungwoon Lee − *Department of Chemistry, Massachusetts Institute of Technology, Cambridge, Massachusetts 02142, United States;* Present Address: Laboratory of Chemical Physics, National Institute of Diabetes and Digestive and Kidney Diseases, National Institutes of Health, Bethesda, Maryland 20892, USA

Mei Hong − *Department of Chemistry, Massachusetts Institute of Technology, Cambridge, Massachusetts 02142, United States;* orcid.org/0000-0001-5255-5858

Complete contact information is available at: https://pubs.acs.org/10.1021/acs.chemmater.2c01795

https://doi.org/10.1021/acs.chemmater.2c01795
Chem. Mater. XXXX, XXX, XXX−XXX

Notes

The authors declare no competing financial interest.

■ ACKNOWLEDGMENTS

The first author thanks the financial support from the 12th Samsung Scholarship Program and Dr. Eugene N. Cho and Prof. Jeffrey C. Grossman for their support in using TGA equipment. This work was supported in part by the MRSEC Program of the National Science Foundation under Award DMR-1419807.

■ REFERENCES

(1) Harrington, M. J.; Masic, A.; Holten-Andersen, N.; Waite, J. H.; Fratzl, P. Iron-Clad Fibers: A Metal-Based Biological Strategy for Hard Flexible Coatings. *Science* **2010**, *328*, 216−220.
(2) Holten-Andersen, N.; Harrington, M. J.; Birkedal, H.; Lee, B. P.; Messersmith, P. B.; Lee, K. Y. C.; Waite, J. H. PH-Induced Metal-Ligand Cross-Links Inspired by Mussel Yield Self-Healing Polymer Networks with near-Covalent Elastic Moduli. *Proc. Natl. Acad. Sci. U.S.A.* **2011**, *108*, 2651−2655.
(3) Filippidi, E.; Cristiani, T. R.; Eisenbach, C. D.; Waite, J. H.; Israelachvili, J. N.; Ahn, B. K.; Valentine, M. T. Toughening Elastomers Using Mussel-Inspired Iron-Catechol Complexes. *Science* **2017**, *358*, 502−505.
(4) Yount, W. C.; Loveless, D. M.; Craig, S. L. Strong Means Slow: Dynamic Contributions to the Bulk Mechanical Properties of Supramolecular Networks. *Angew. Chem.* **2005**, *117*, 2806−2808.
(5) Lee, B. P.; Messersmith, P. B.; Israelachvili, J. N.; Waite, J. H. Mussel-Inspired Adhesives and Coatings. *Annu. Rev. Mater. Res.* **2011**, *41*, 99−132.
(6) Degtyar, E.; Harrington, M. J.; Politi, Y.; Fratzl, P. The Mechanical Role of Metal Ions in Biogenic Protein-Based Materials. *Angew. Chem., Int. Ed.* **2014**, *53*, 12026−12044.
(7) Holten-Andersen, N.; Jaishankar, A.; Harrington, M. J.; Fullenkamp, D. E.; DiMarco, G.; He, L.; McKinley, G. H.; Messersmith, P. B.; Lee, K. Y. C. Metal-Coordination: Using One of Nature's Tricks to Control Soft Material Mechanics. *J. Mater. Chem. B* **2014**, *2*, 2467−2472.
(8) Zhong, Q.; Richardson, J. J.; Li, S.; Zhang, W.; Ju, Y.; Li, J.; Pan, S.; Chen, J.; Caruso, F. Expanding the Toolbox of Metal−Phenolic Networks via Enzyme-Mediated Assembly. *Angew. Chem.* **2020**, *132*, 1728−1734.
(9) Zhang, C.; Wu, B.; Zhou, Y.; Zhou, F.; Liu, W.; Wang, Z. Mussel-Inspired Hydrogels: From Design Principles to Promising Applications. *Chem. Soc. Rev.* **2020**, *49*, 3605−3637.
(10) Lichtenegger, H. C.; Schöberl, T.; Ruokolainen, J. T.; Cross, J. O.; Heald, S. M.; Birkedal, H.; Waite, J. H.; Stucky, G. D. Zinc and Mechanical Prowess in the Jaws of Nereis, a Marine Worm. *Proc. Natl. Acad. Sci. U.S.A.* **2003**, *100*, 9144−9149.
(11) Lichtenegger, H. C.; Schöberl, T.; Bartl, M. H.; Waite, H.; Stucky, G. D. High Abrasion Resistance with Sparse Mineralization: Copper Biomineral in Worm Jaws. *Science* **2002**, *298*, 389−392.
(12) Broomell, C. C.; Mattoni, M. A.; Zok, F. W.; Waite, J. H. Critical Role of Zinc in Hardening of Nereis Jaws. *J. Exp. Biol.* **2006**, *209*, 3219−3225.
(13) Khan, R. K.; Stoimenov, P. K.; Mates, T. E.; Waite, J. H.; Stucky, G. D. Exploring Gradients of Halogens and Zinc in the Surface and Subsurface of Nereis Jaws. *Langmuir* **2006**, *22*, 8465−8471.
(14) Stewart, R. J.; Ransom, T. C.; Hlady, V. Natural Underwater Adhesives. *J. Polym. Sci., Part B: Polym. Phys.* **2011**, *49*, 757−771.
(15) Carrington, E.; Gosline, J. M. Mechanical Design of Mussel Byssus: Load Cycle and Strain Rate Dependence. *Am. Malacological Bull.* **2004**, *18*, 135−142.
(16) Waite, J. H.; Qin, X. X.; Coyne, K. J. The Peculiar Collagens of Mussel Byssus. *Matrix Biol.* **1998**, *17*, 93−106.
(17) Harrington, M. J.; Waite, J. H. Holdfast Heroics: Comparing the Molecular and Mechanical Properties of Mytilus Californianus Byssal Threads. *J. Exp. Biol.* **2007**, *210*, 4307−4318.
(18) Holten-Andersen, N.; Fantner, G. E.; Hohlbauch, S.; Waite, J. H.; Zok, F. W. Protective Coatings on Extensible Biofibres. *Nat. Mater.* **2007**, *6*, 669−672.
(19) Holten-Andersen, N.; Zhao, H.; Waite, J. H. Stiff Coatings on Compliant Biofibers: The Cuticle of Mytilus Californianus Byssal Threads. *Biochemistry* **2009**, *48*, 2752−2759.
(20) Holten-Andersen, N.; Mates, T. E.; Toprak, M. S.; Stucky, G. D.; Zok, F. W.; Waite, J. H. Metals and the Integrity of a Biological Coating: The Cuticle of Mussel Byssus. *Langmuir* **2009**, *25*, 3323−3326.
(21) Sun, C.; Waite, J. H. Mapping Chemical Gradients within and along a Fibrous Structural Tissue, Mussel Byssal Threads. *J. Biol. Chem.* **2005**, *280*, 39332−39336.
(22) Hwang, D. S.; Harrington, M. J.; Lu, Q.; Masic, A.; Zeng, H.; Waite, J. H. Mussel Foot Protein-1 (Mcfp-1) Interaction with Titania Surfaces. *J. Mater. Chem.* **2012**, *22*, 15530−15533.
(23) Yu, J.; Wei, W.; Menyo, M. S.; Masic, A.; Waite, J. H.; Israelachvili, J. N. Adhesion of Mussel Foot Protein-3 to TiO2 Surfaces: The Effect of PH. *Biomacromolecules* **2013**, *14*, 1072−1077.
(24) Lee, H.; Scherer, N. F.; Messersmith, P. B. Single-Molecule Mechanics of Mussel Adhesion. *Proc. Natl. Acad. Sci. U.S.A.* **2006**, *103*, 12999−13003.
(25) Hwang, D. S.; Zeng, H.; Masic, A.; Harrington, M. J.; Israelachvili, J. N.; Waite, J. H. Protein- and Metal-Dependent Interactions of a Prominent Protein in Mussel Adhesive Plaques. *J. Biol. Chem.* **2010**, *285*, 25850−25858.
(26) Yount, W. C.; Juwarker, H.; Craig, S. L. Orthogonal Control of Dissociation Dynamics Relative to Thermodynamics in a Main-Chain Reversible Polymer. *J. Am. Chem. Soc.* **2003**, *125*, 15302−15303.
(27) Geng, H.; Zhong, Q.-Z.; Li, J.; Lin, Z.; Cui, J.; Caruso, F.; Hao, J. Metal Ion-Directed Functional Metal−Phenolic Materials. *Chem. Rev.* **2022**, *122*, 11432−11473.
(28) Carrington, E.; Waite, J. H.; Sarà, G.; Sebens, K. P. Mussels as a Model System for Integrative Ecomechanics. *Annu. Rev. Mar. Sci.* **2015**, *7*, 443−469.
(29) Carrington, E. Seasonal Variation in the Attachment Strength of Blue Mussels: Causes and Consequences. *Limnol. Oceanogr.* **2002**, *47*, 1723−1733.
(30) Carrington, E. The Ecomechanics of Mussel Attachment: From Molecules to Ecosystems. *Integr. Comp. Biol.* **2002**, *42*, 846−852.
(31) Monnier, C. A.; DeMartini, D. G.; Waite, J. H. Intertidal Exposure Favors the Soft-Studded Armor of Adaptive Mussel Coatings. *Nat. Commun.* **2018**, *9*, No. 3424.
(32) Kim, S.; Peterson, A. M.; Holten-Andersen, N. Enhanced Water Retention Maintains Energy Dissipation in Dehydrated Metal-Coordinate Polymer Networks: Another Role for Fe-Catechol Cross-Links? *Chem. Mater.* **2018**, *30*, 3648−3655.
(33) Fullenkamp, D. E.; He, L.; Barrett, D. G.; Burghardt, W. R.; Messersmith, P. B. Mussel-Inspired Histidine-Based Transient Network Metal Coordination Hydrogels. *Macromolecules* **2013**, *46*, 1167−1174.
(34) Grindy, S. C.; Learsch, R.; Mozhdehi, D.; Cheng, J.; Barrett, D. G.; Guan, Z.; Messersmith, P. B.; Holten-Andersen, N. Control of Hierarchical Polymer Mechanics with Bioinspired Metal-Coordination Dynamics. *Nat. Mater.* **2015**, *14*, 1210−1216.
(35) Fullenkamp, D. E.; Barrett, D. G.; Miller, D. R.; Kurutz, J. W.; Messersmith, P. B. PH-Dependent Cross-Linking of Catechols through Oxidation via Fe(3+) and Potential Implications for Mussel Adhesion. *RSC Adv.* **2014**, *4*, 25127−25134.
(36) Barrett, D. G.; Fullenkamp, D. E.; He, L. H.; Holten-Andersen, N.; Lee, K. Y. C.; Messersmith, P. B. PH-Based Regulation of Hydrogel Mechanical Properties through Mussel-Inspired Chemistry and Processing. *Adv. Funct. Mater.* **2013**, *23*, 1111−1119.
(37) Li, Q.; Barrett, D. G.; Messersmith, P. B.; Holten-andersen, N. Controlling Hydrogel Mechanics via Bio-Inspired Polymer−Nanoparticle Bond Dynamics. *ACS Nano* **2016**, *10*, 1317−1324.

https://doi.org/10.1021/acs.chemmater.2c01795
Chem. Mater. XXXX, XXX, XXX−XXX

(38) Palmer, R. G.; Stein, D. L.; Abrahams, E.; Anderson, P. W. Models of Hierarchically Constrained Dynamics for Glassy Relaxation. *Phys. Rev. Lett.* **1984**, *53*, 958−961.
(39) Cathébras, N.; Collet, A.; Viguier, M.; Berret, J. F. Synthesis and Linear Viscoelasticity of Fluorinated Hydrophobically Modified Ethoxylated Urethanes (F-HEUR). *Macromolecules* **1998**, *31*, 1305−1311.
(40) Jarzcki, A. A.; Anbar, A. D.; Spiro, T. G. DFT Analysis of Fe(H 2 O) 6 3+ and Fe(H 2 O) 6 2+ Structure and Vibrations; Implications for Isotope Fractionation. *J. Phys. Chem. A* **2004**, *108*, 2726−2732.
(41) Best, S. P.; Beattie, J. K.; Armstrong, R. S. Vibrational Spectroscopic Studies of Trivalent Hexa-Aqua-Cations: Single-Crystal Raman Spectra between 275 and 1 200 Cm^{-1} of the Caesium Alums of Titanium, Vanadium, Chromium, Iron, Gallium, and Indium. *J. Chem. Soc., Dalton Trans.* **1984**, *12*, 2611−2624.
(42) Schmitt, C. N. Z.; Winter, A.; Bertinetti, L.; Masic, A.; Strauch, P.; Harrington, M. J. Mechanical Homeostasis of a DOPA-Enriched Biological Coating from Mussels in Response to Metal Variation. *J. R. Soc. Interface* **2015**, *12*, No. 20150466.
(43) Gottlieb, H. E.; Kotlyar, V.; Nudelman, A. NMR Chemical Shifts of Common Laboratory Solvents as Trace Impurities. *J. Org. Chem.* **1997**, *62*, 7512−7515.
(44) Fulmer, G. R.; Miller, A. J. M.; Sherden, N. H.; Gottlieb, H. E.; Nudelman, A.; Stoltz, B. M.; Bercaw, J. E.; Goldberg, K. I. NMR Chemical Shifts of Trace Impurities: Common Laboratory Solvents, Organics, and Gases in Deuterated Solvents Relevant to the Organometallic Chemist. *Organometallics* **2010**, *29*, 2176−2179.
(45) Lee, M.; Hong, M. Cryoprotection of Lipid Membranes for High-Resolution Solid-State NMR Studies of Membrane Peptides and Proteins at Low Temperature. *J. Biomol. NMR* **2014**, *59*, 263−277.
(46) White, P. B.; Wang, T.; Park, Y. B.; Cosgrove, D. J.; Hong, M. Water−Polysaccharide Interactions in the Primary Cell Wall of *Arabidopsis Thaliana* from Polarization Transfer Solid-State NMR. *J. Am. Chem. Soc.* **2014**, *136*, 10399−10409.
(47) Li, C. H.; Wang, C.; Keplinger, C.; Zuo, J. L.; Jin, L.; Sun, Y.; Zheng, P.; Cao, Y.; Lissel, F.; Linder, C.; You, X. Z.; Bao, Z. A Highly Stretchable Autonomous Self-Healing Elastomer. *Nat. Chem.* **2016**, *8*, 618−624.
(48) Rao, Y.-L.; Chortos, A.; Pfattner, R.; Lissel, F.; Chiu, Y.-C.; Feig, V.; Xu, J.; Kurosawa, T.; Gu, X.; Wang, C.; He, M.; Won Chung, J.; Bao, Z. Stretchable Self-Healing Polymeric Dielectrics Cross-Linked Through Metal−Ligand Coordination. *J. Am. Chem. Soc.* **2016**, *138*, 6020−6027.
(49) Yount, W. C.; Loveless, D. M.; Craig, S. L. Small-Molecule Dynamics and Mechanisms Underlying the Macroscopic Mechanical Properties of Coordinatively Cross-Linked Polymer Networks. *J. Am. Chem. Soc.* **2005**, *127*, 14488−14496.
(50) Laage, D.; Elsaesser, T.; Hynes, J. T. Water Dynamics in the Hydration Shells of Biomolecules. *Chem. Rev.* **2017**, *117*, 10694−10725.
(51) Badger, J. Multiple Hydration Layers in Cubic Insulin Crystals. *Biophys. J.* **1993**, *65*, 1656−1659.
(52) Kaur, S.; Narayanan, A.; Dalvi, S.; Liu, Q.; Joy, A.; Dhinojwala, A. Direct Observation of the Interplay of Catechol Binding and Polymer Hydrophobicity in a Mussel-Inspired Elastomeric Adhesive. *ACS Cent. Sci.* **2018**, *4*, 1420−1429.
(53) Gómez-Zaleta, B.; Gómez-Balderas, R.; Hernández-Trujillo, J. Theoretical Analysis of Hydrogen Bonding in Catechol-n(H2O) Clusters (n = 0···3). *Phys. Chem. Chem. Phys.* **2010**, *12*, 4783−4790.
(54) Eloi, J.-C.; Chabanne, L.; Whittell, G. R.; Manners, I. Metallopolymers with Emerging Applications. *Mater. Today* **2008**, *11*, 28−36.
(55) Bellarosa, L.; García-Muelas, R.; Revilla-López, G.; López, N. Diversity at the Water−Metal Interface: Metal, Water Thickness, and Confinement Effects. *ACS Cent. Sci.* **2016**, *2*, 109−116.
(56) Yun, G.; Richardson, J. J.; Biviano, M.; Caruso, F. Tuning the Mechanical Behavior of Metal−Phenolic Networks through Building Block Composition. *ACS Appl. Mater. Interfaces* **2019**, *11*, 6404−6410.
(57) Ejima, H.; Richardson, J. J.; Caruso, F. Metal-Phenolic Networks as a Versatile Platform to Engineer Nanomaterials and Biointerfaces. *Nano Today* **2017**, 136−148.
(58) Wilt, J. K.; Gilmer, D.; Kim, S.; Compton, B. G.; Saito, T. Direct Ink Writing Techniques for in Situ Gelation and Solidification. *MRS Commun.* **2021**, *11*, 106−121.
(59) Priemel, T.; Palia, G.; Förste, F.; Jehle, F.; Sviben, S.; Mantouvalou, I.; Zaslansky, P.; Bertinetti, L.; Harrington, M. J. Microfluidic-like Fabrication of Metal Ion−Cured Bioadhesives by Mussels. *Science* **2021**, *374*, 206−211.

NOTE ADDED AFTER ASAP PUBLICATION

Due to a production error, this paper was published ASAP on November 30, 2022, with an error in the Figure 3 caption. The corrected version was reposted on December 1, 2022.

https://doi.org/10.1021/acs.chemmater.2c01795
Chem. Mater. XXXX, XXX, XXX−XXX

Supporting Information

Quantitative Correlation between Bound Water and Mechanical Stress-relaxation in Dehydrated Metal-Coordinate Polymer Networks

By *Sungjin Kim,* [a,+]* *Myungwoon Lee,* [b,++] *Mei Hong*[b] and *Niels Holten-Andersen*[a,+++]*

[a] Dr. S. Kim, Prof. N. Holten-Andersen
Department of Materials Science and Engineering
Massachusetts Institute of Technology
Cambridge, MA 02142, United States of America

[b] Dr. M. Lee, Prof. M. Hong
Department of Chemistry
Massachusetts Institute of Technology
Cambridge, MA 02142, United States of America

* Correspondence to kims1@ornl.gov, nih221@lehigh.edu

[+]present affiliation: Chemical Sciences Division, Oak Ridge National Laboratory, Oak Ridge, TN 37831, USA

[++]present affiliation: Laboratory of Chemical Physics, National Institute of Diabetes and Digestive and Kidney Diseases, National Institutes of Health, Bethesda, MD 20892, USA

[+++]present affiliation: Department of Materials Science and Engineering, Department of Bioengineering, Lehigh University, Bethlehem, PA 18015, USA

Supporting Information contains:

Figure S1-S10

Table S1-S4

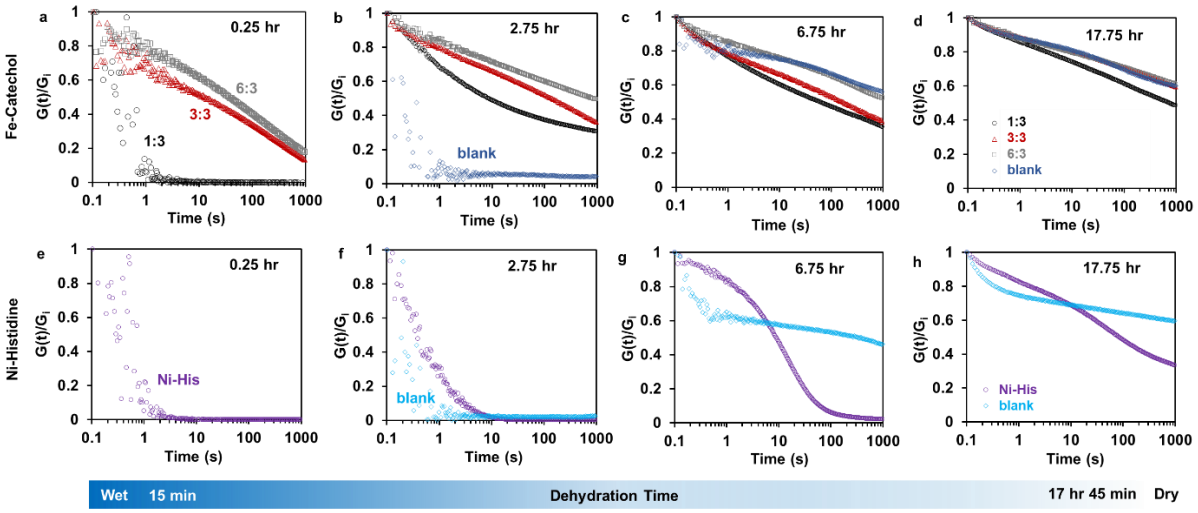

Figure S1

Step-strain (at strain of 10 %) relaxation curves of (a-d) Fe-catechol systems with different Fe:catechol ratios (1:3 - black circles, 3:3 - red triangles, 6:3 - gray squares) or without metals (blank - blue diamonds), and (e-h) those of Ni-histidine systems with Ni:His ratio of 1:2 (Ni-His, purple circles) or without metals (blank – light blue diamonds) after (a, e) 0.25, (b, f) 2.75, (c, g) 6.75, and (d, h) 17.75 hours of dehydration (R.H. 16 %, 25 °C). G(t) is normalized by G_i (the initial modulus) at 0.1 sec when the strain stabilized at the set value. For convenience, we labeled the system after 0.25 hrs as H (hydrated) and that after 17.75 hours as D (dehydrated) in Figure 1e. The metal-coordination-dominant network (1:3) visibly shows the fastest relaxation throughout the total 17.75 hours of dehydration (Figure S1a-d) among the Fe-catechol networks. It is notable that after dehydrating for 6.75 hours, the Fe-coordinate gels showed faster relaxation than the metal-free (blank) 4cPEG solution (Figure S1c) which was liquid at 0.25 hours (Figure S1a), and the fastest-relaxing catechol system until the 2.75 hours of dehydration (Figure S1b). These observations indicate that the metal-coordination bonds stayed dynamic even after long dehydration of ~18 hours, whereas such dehydration has induced a significant physical interaction between the polymer chains, making the blank system behave close to a covalent-dominant network. Similar phenomena were also observed in Ni-histidine networks (Figure S1e-h). The metal-free (blank) 4hPEG, like the blank 4cPEG system, was unable to show the viscoelastic stress-relaxation at 0.25 hours of dehydration as a liquid state (Figure S1e). After 6.75 hours of dehydration, the Ni-histidine gel clearly displayed faster stress-relaxation than the blank 4hPEG (Figure S1g, S1h). These trends of the Ni-histidine system agree well with the metal-coordination-dominant 1:3 system.

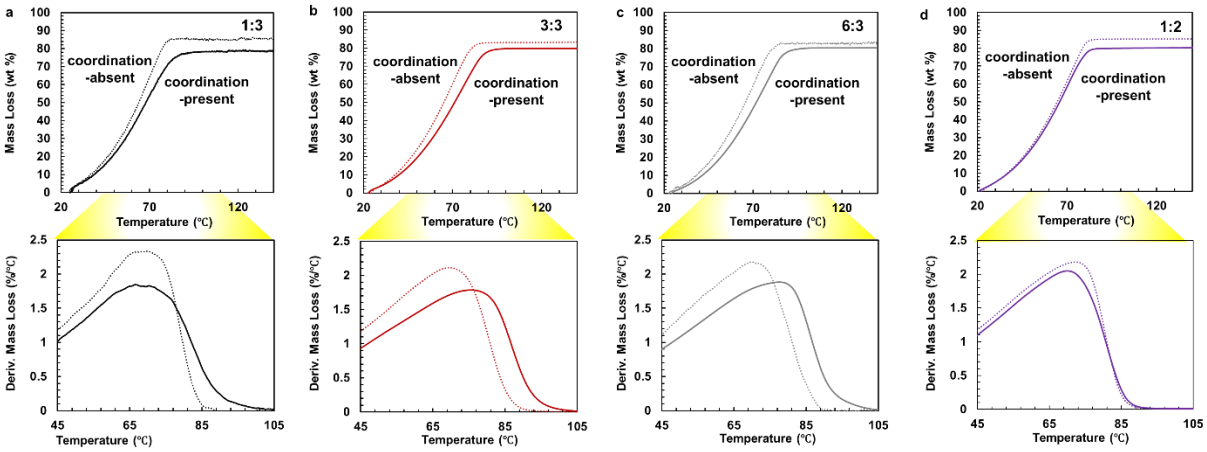

Figure S2

(a-d) Thermogravimetric analysis (TGA, upper row) and derivative thermogravimetric analysis (DTG, lower row) on Fe-catechol system with Fe:catechol ratios of (a) 1:3 (solid black), (b) 3:3 (solid red), (c) 6:3 (solid gray) and (d) on Ni-his system (Ni:histidine=1:2, solid purple). For comparison, identical tests were performed on coordination-absent samples of each corresponding composition of metal ions and polymer without the metal-coordinating ligands (i.e., catechols or histidines) (dotted).

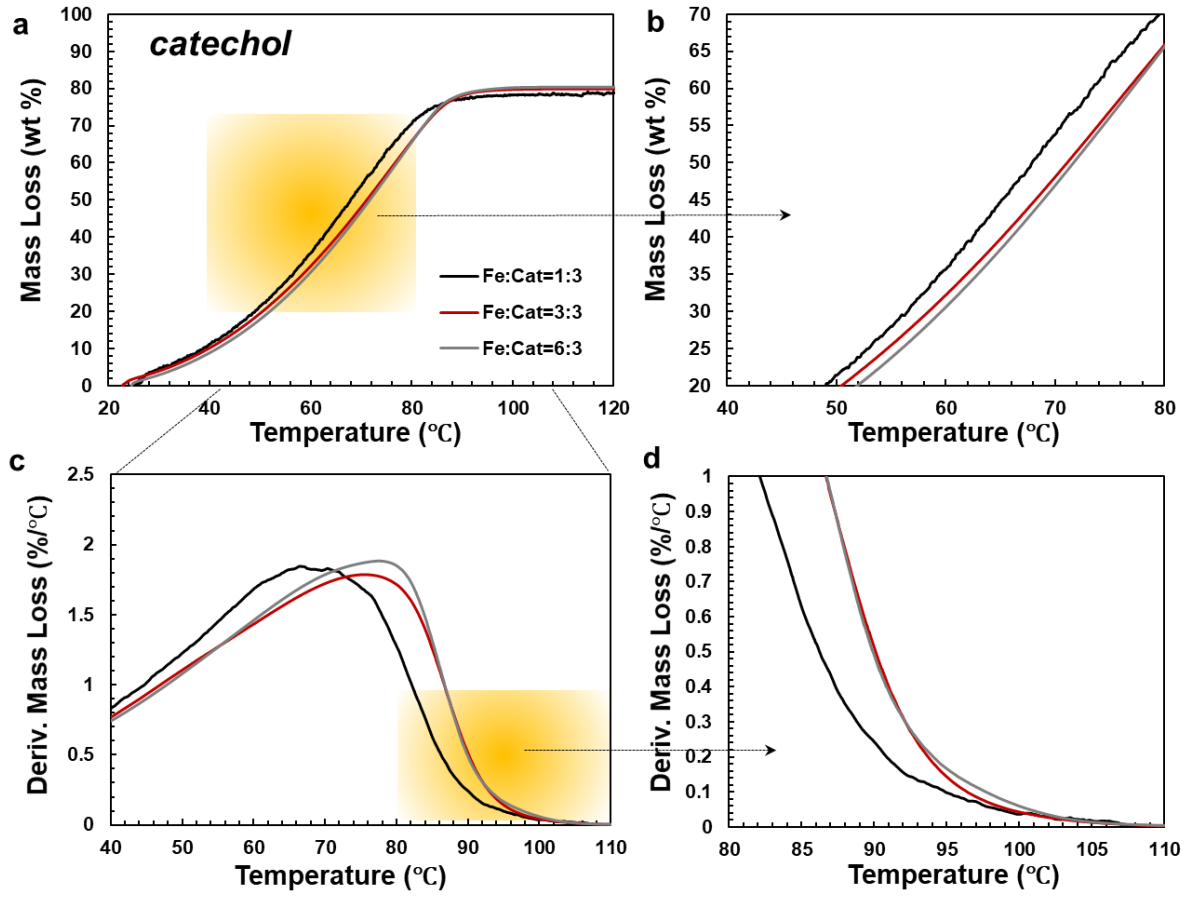

Figure S3

Comparison of Fe-catechol-coordination-present systems (with catechol ligands) with Fe:catechol = 1:3 (black), 3:3 (red), and 6:3 (gray) upon thermal increment in TGA. (a) The TGA profile from 20 to 120 ℃ and (b) that in the focused region of temperature ranging from 40 to 80 ℃ and mass loss ranging from 20 to 70 wt % for better visual comparison. (c) DTG profile from 40 to 110 ℃ and (d) that in the more focused range from 80 to 110 ℃ where mass loss rates of all samples reach ~ 0. Note that the 1:3 (the most coordination-dominant network) shows the lowest water loss as seen in (a). Although the 1:3 tends to show earlier mass loss upon heating (b, c) as expected for the lowest amount of solutes, the maximum mass loss rate (c, ~ 1.9 %/℃) and the temperature at maximum dehydration (d, ~ 110 ℃) are similar to the samples with more solutes (i.e., 3:3 and 6:3).

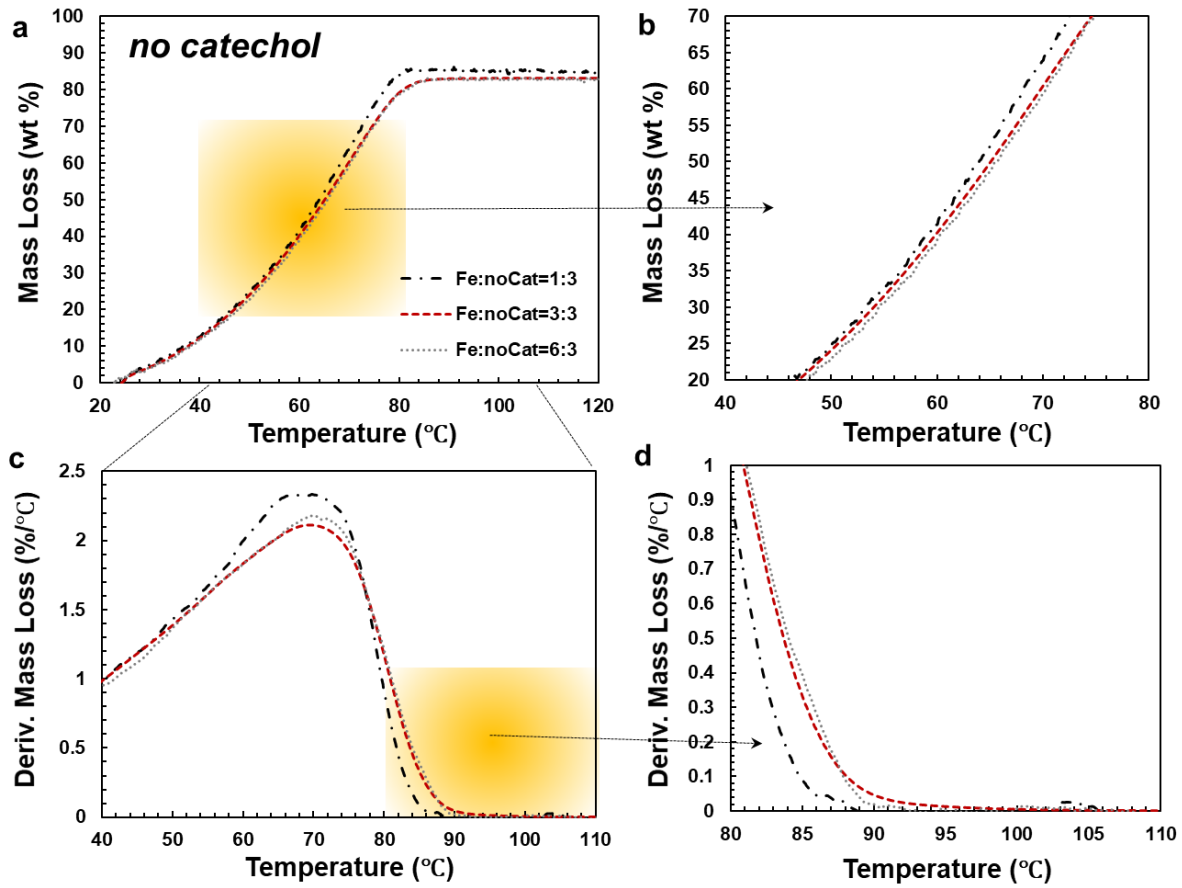

Figure S4

Comparison of Fe-catechol-coordination-absent systems (without catechol ligands) with Fe:catechol = 1:3 (dash-dotted black), 3:3 (dashed red), and 6:3 (dotted gray) upon thermal increment in TGA. (a) The TGA profile from 20 to 120 ℃ and (b) that in the focused region of temperature ranging from 40 to 80 ℃ and mass loss ranging from 20 to 70 wt % for better visual comparison. (c) The DTG profile from 40 to 110 ℃ and (d) in the more focused range from 80 to 110 ℃ where mass loss rates of all samples reach ~0. In contrast to the Fe-catechol-present systems, the 1:3 shows the highest (a) and the earliest (b, c) water loss upon heating, the fastest maximum water loss rate (c, ~2.4 %/℃), and the lowest temperature for reaching the maximum dehydration (d, ~ 90 ℃) as normally expected for a general solution with the least amount of solutes.

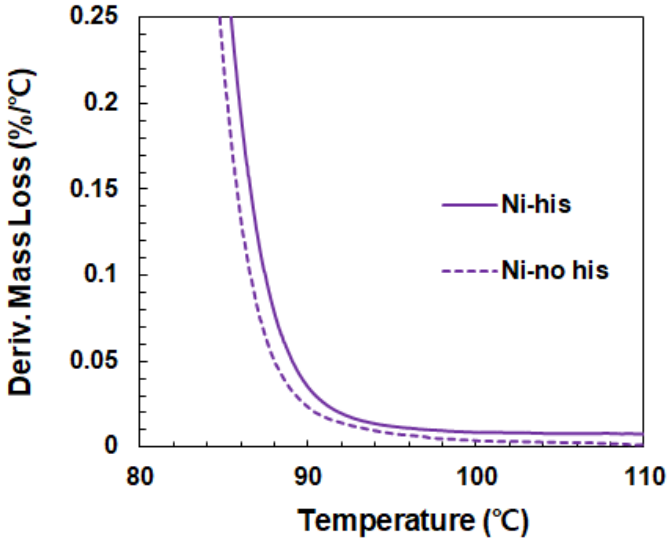

Figure S5

DTG profiles of Ni-histidine systems with or without the histidine ligands in the focused range from 80 to 110 °C from Figure S2d (lower panel) for a better visual comparison. The Ni-his-coordination-present system holds onto the water for higher temperatures than the coordination-absent system.

Approx. Raman Shift (cm^{-1})	*Assignment*	*Present in*
320	O-Fe-O stretching from Fe-H_2O interaction	1:3 (strong) 3:3 (medium) 6:3 (weak)
530	charge-transfer interaction from bidentate chelate of catechols	all
590, 635	interaction between the Fe and O from catechols	all
1250 – 1480	aromatic ring vibrations	all

Table S1

Assignment of the observed Raman peaks in Figure 2c. The three samples (1:3, 3:3, 6:3) show different sharpness and relative intensity of vibration band corresponding to the O-Fe-O deformation at ~320 cm^{-1} attributed to the Fe-H_2O interaction from H_2O possibly filling positions in the first coordination shell.[1–3] This peak at ~320 cm^{-1} is shown to be most eminent in 1:3 whereas the peak became blunt and insignificant in 6:3. Phenyl ring vibrations from ~1250 to ~1480 cm^{-1} are present in all three samples. The three samples all show the characteristic peaks for Fe-catechol coordinations: the distinct coordination peaks at ~ 590 and ~ 635 cm^{-1} attributed to the interactions between the Fe^{3+} and the oxygen of catechols and the peak at ~ 530 cm^{-1} attributed to the charge transfer interaction from bidentate chelates.

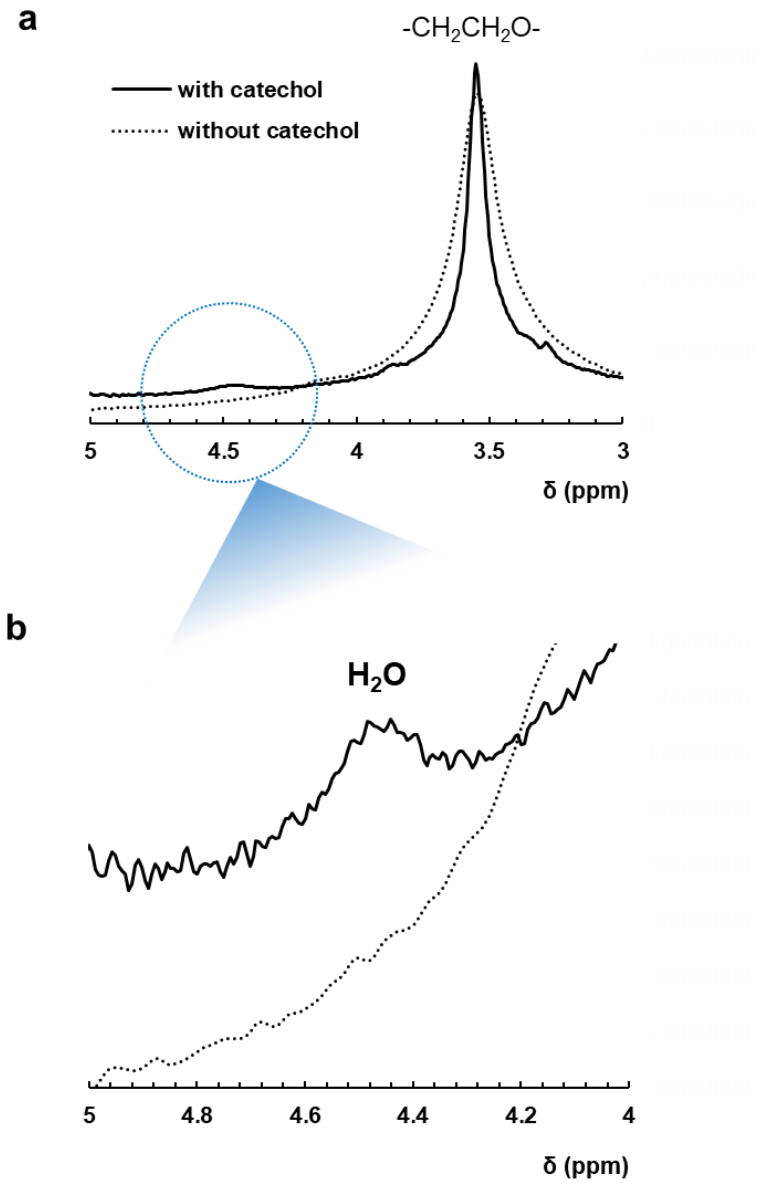

Figure S6

^{1}H-NMR analyses on the systems with Fe:catechol ratio of 1:3 dehydrated at 20 ℃ over 48 hours in 16 % R.H.. (a) The spectra for the system with catechol moieties that coordinate Fe (solid line) and those without catechol moieties (dotted line). (b) The spectra zoomed in around the peak at δ ~ 4.4 ppm which corresponds to protons in H_2O.[4–7] It indicates that there exist mobile H_2O molecules responsive to the applied magnetic field among the high amount of water retained in the 1:3 system. The peak at δ ~ 3.5 corresponds to the -CH_2CH_2O- of PEG.[8]

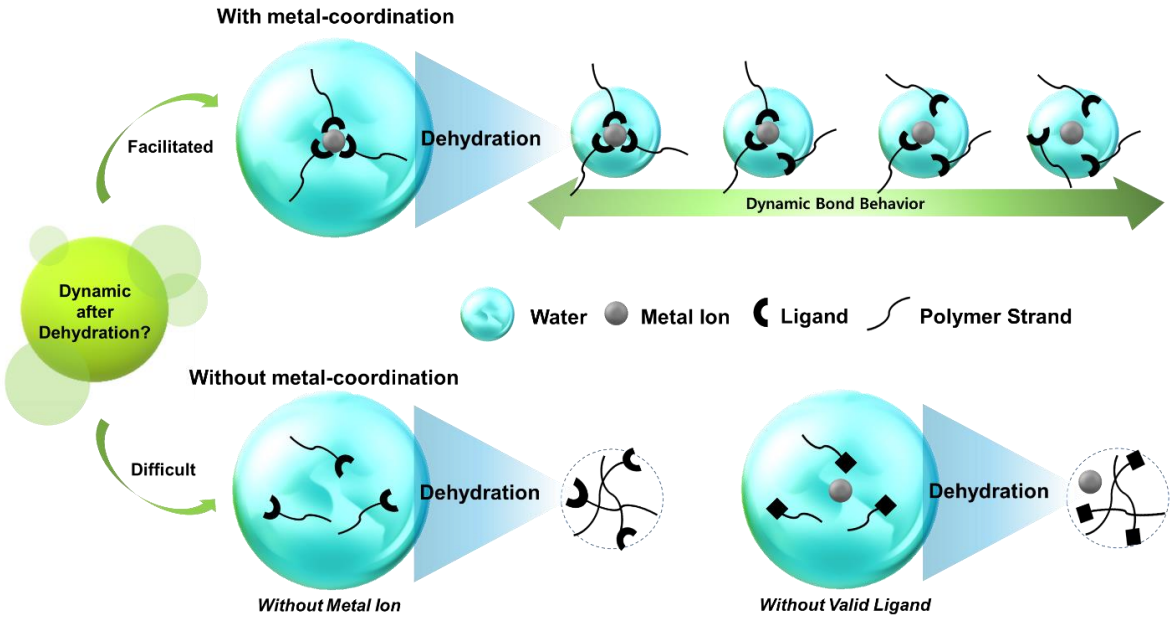

Figure S7
The schematic figure depicting metal-coordinate bonds retaining water which facilitates the dynamic metal-coordinate bond behaviors after dehydration. The uncrosslinked, coordination-free systems, without either the metal ions or the metal-binding ligands, hardly retain water after dehydration and become significantly non-dynamic compared with the metal-coordinate-rich systems with water retention.

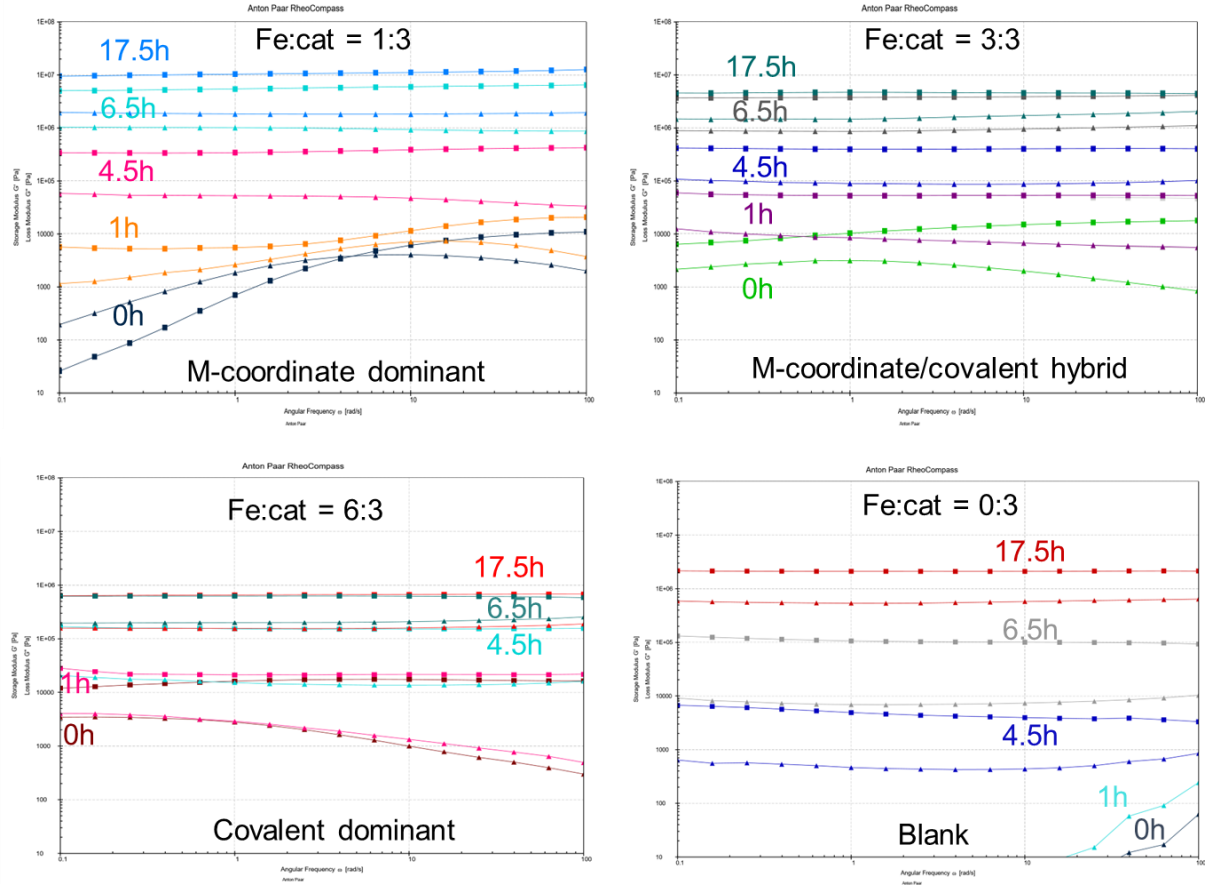

Figure S8

The frequency sweep profiles of 1:3, 3:3, 6:3, and 0:3 (blank) throughout the 17.5 hours of dehydration. While the relaxation time determined by the crossover between the G' (squares) and G" (triangles) could not be captured within the measured timeframe except for the 1:3 after 0 hours of dehydration, the current results show that the network ends up stiffer after dehydration as the metal-coordinate bonds dominate over the covalent bonds in the system. This result agrees well with the observations in the previous report that the metal-coordinate network ends up stiffer than the perfectly covalent catecholic network after dehydration.[9] While the detailed mechanistic discussion for these stiffening phenomena would be out of the main scope of this paper, this observation implies that the tris-metal-coordination bonds with higher functionality than dicatecholic covalent bonds, as well as the dehydration-induced physical interactions, contribute to the effective crosslink density of the dehydrated network. This supposition is further supported by the previous report suggesting that the metal-catechol ionic complexes aggregate upon dehydration to form concentrated metal ion clusters, which may further increase the functionality of the crosslinks.[10] In contrast, the dicatecholic covalent crosslink-dominant network has fewer high-functionality catechol-metal complexes (and their clusters) and fewer uncrosslinked or dynamically dissociated free polymer strands that can easily form effective physical crosslinks induced upon dehydration. The latter point is also supported by that the blank crosslink-free system ends up stiffer by dehydration than the covalent-dominant 6:3 system. Thereby, the covalent-dominant network ends up rather compliant compared with other systems. Hence, these results support that the metal-coordinate bonds still contribute to the network elasticity after dehydration.

System	Metal ion (μmol)	Ligand (μmol)	M-Coordination complex $\mathbf{n_{complex}}$ (μmol)	Bound water $\mathbf{n_{H2O}}$ (μmol) from fig. 2	Number of bound water per complex $\underline{\mathbf{n_{H2O}}}$ = $n_{H2O}/n_{complex}$	Note * *italicized values* are more likely
Fe:catechol = 1:3	0.3	1	0.3	84.26	*281*	All Fe ions are forming tris-Fe-catechol coordination complexes
Fe:catechol = 3:3	1	1	*0.15* ≤ $n_{complex}$ < 0.3	42.32	141 < $\underline{n_{H2O}}$ ≤ *281*	Covalently pre-crosslinked catechols do not participate in coordination as effectively as free catechols
Fe:catechol = 6:3	2	1	*0.12* ≤ $n_{complex}$ < 0.3	33.08	110 < $\underline{n_{H2O}}$ ≤ *281*	Covalently pre-crosslinked catechols do not participate in coordination as effectively as free catechols
Ni:histidine = 1:2	0.5	1	0.5	63.96	128	All Ni ions are forming bis-Ni-histidine coordination complexes

Table S2

The table showing the number of metal ions, ligands, metal-coordination complexes ($n_{complex}$), bound water molecules (n_{H2O} from Figure 2b), and bound water molecules per complex ($\underline{n_{H2O}}$) in each system. The $\underline{n_{H2O}}$ is calculated by dividing the n_{H2O} (in Figure 2b) by the $n_{complex}$. Here, we assume that every Fe^{3+} in the Fe:catechol = 1:3 system and every Ni^{2+} in the Ni:histidine = 1:2 system function as a coordination center in the respective metal-coordination complex (i.e., the number of metal ions = $n_{complex}$). Then, the $n_{complex}$ of the Fe:catechol = 3:3 or 6:3 is expected to be lower than that of 1:3 (i.e., 0.3 μmol) since the catechols pre-crosslinked covalently by the excess Fe^{3+} in the former two systems are unlikely to participate in coordination as effectively as the free catechols.[11] Hence, we set the lower limit of the $\underline{n_{H2O}}$ for 3:3 and 6:3 systems as the $\underline{n_{H2O}}$ when all catechols are still available to coordinate with 0.3 μmol of Fe^{3+} in each system (which is unlikely as stated previously), and the upper limit as the $\underline{n_{H2O}}$ of 1:3 that has the most bound water (then we can back-calculate the lower limit of $n_{complex}$ – italicized). We consider that $\underline{n_{H2O}}$ of all Fe-catechol systems are the same (i.e., 281 – italicized) because (i) the type of metal and ligand forming the coordination complex stays the same and (ii) it is reasonable to expect $n_{complex}$, instead of $\underline{n_{H2O}}$, to decline as more catechols are oxidized for covalent pre-coupling as [Fe^{3+}] increases (Figure 1a). Regardless, all estimated $\underline{n_{H2O}}$ indicate the existence of multiple hydration layers per complex in every given system.

System Label	1	2	3
Fe:catechol	1:3	3:3	6:3
τ (sec)	136.49	3150.58	13215.47
n_{H2O} (μmol)	84.26	42.32	33.08

Table S3

The table of Fe-catechol systems (Fe:catechol = 1:3, 3:3, 6:3) with their relaxation times (τ) after 17.75 hours of dehydration at 25 ℃ at 16 % R.H. from Figure 1 and n_{H_2O} from Figure 2b. The given systems are labeled as 1, 2, and 3 for convenience in mathematical modeling (Figure 4, Table S4, Figure S9, S10).

Selected Systems Labels from Table S3	**Δn_{H2O} = n_{H2O} (b) - n_{H2O} (a)**	**τ_a/τ_b** Experimental from Table S3	**Fitting Information**	**τ_a/τ_b** Fitted Ver. 1	**τ_a/τ_b** Fitted Ver. 2
			Fitting Formula	y = exp(kx)	y = π^x
				y = π^x (converted)	
			R^2	0.9802	0.9547
			k	0.0849	n/a
			π	1.0886 (converted)	1.0920
			Software	MS Excel 2016	OriginPro 8
a=1, b=3	-51.1887	0.0103	Fitted Values	0.0130	0.0110
a=1, b=2	-41.9397	0.0433		0.0284	0.0249
a=2, b=3	-9.2490	0.2384		0.4560	0.4429
a=3, b=2	9.2490	4.1946		2.1929	2.2577
a=2, b=1	41.9397	23.0835		35.1872	40.1526
a=3, b=1	51.1887	96.8264		77.1634	90.6532

Table S4

The table showing the detailed information and data for the Δn_{H_2O} (x-axis) versus τ_a/τ_b (y-axis) graph in Figure 4. The pairs from Fe-catechol systems from Table S3 are selected to produce parameters for numerical correlation using our model (Table S2, Figure S7). Two exponential fitting formulas of y = exp(kx) (Ver. 1, k is a constant determined by the fitting process) and y = π^x (Ver. 2) were used to estimate the values. The Ver. 1 was later converted to the form of y = π^x for direct comparison after the fitting process. The two versions are plotted in comparison in Figure S9. The Ver. 1 with a higher R^2 value is displayed in the main manuscript (Figure 4).

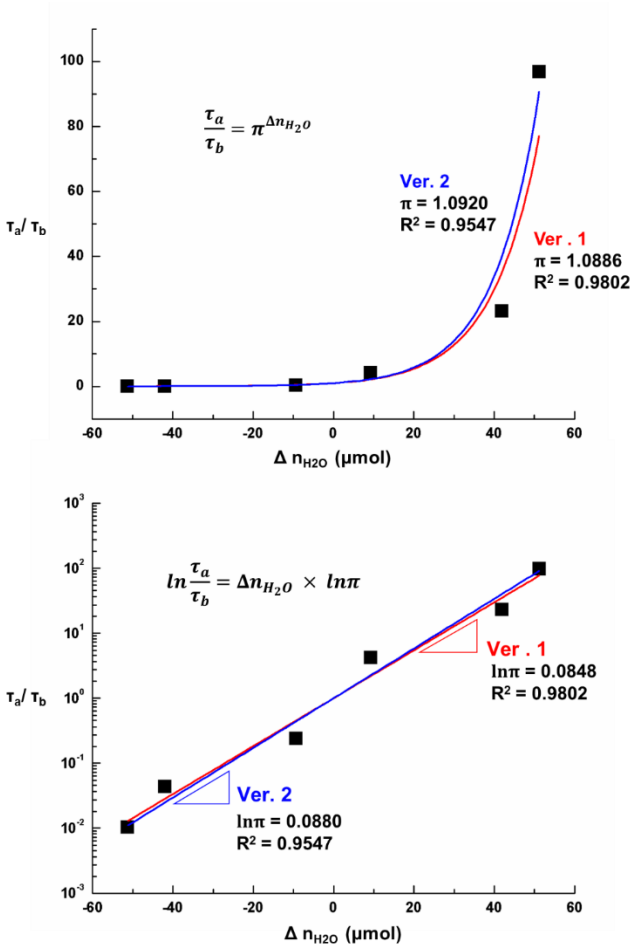

Figure S9

The plot showing the Δn_{H_2O} versus τ_a/τ_b in the linear (upper) and logarithmic (lower) scale of our obtained data and fitted curves from each fitting method Ver.1 (red) and Ver. 2 (blue) from Table S4. Both methods prove the exponential relation between the dynamic behavior of the network (represented by τ_a/τ_b) and the number of retained water molecules (Δn_{H_2O}).

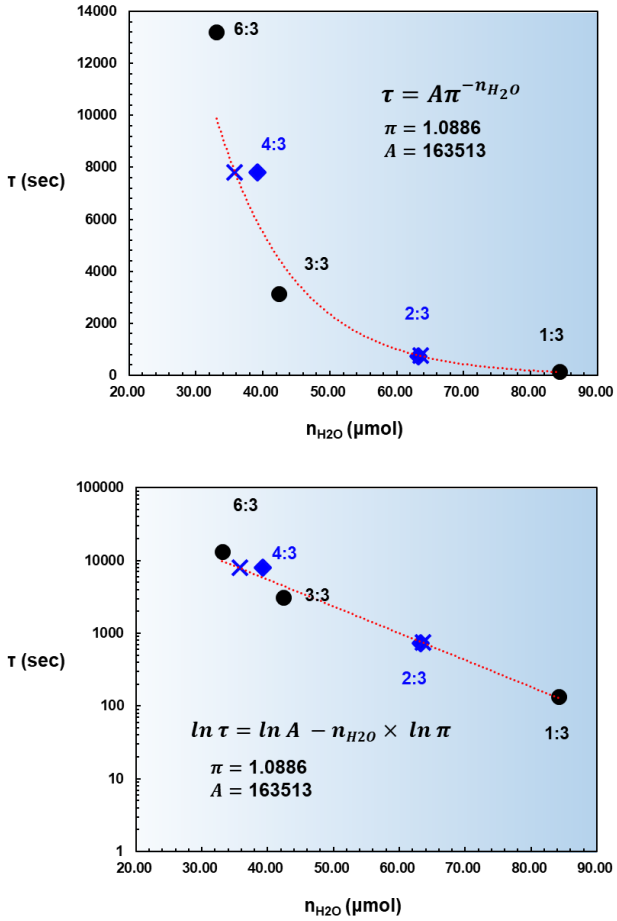

Figure S10

The plot showing n_{H_2O} versus τ in the linear (upper) and logarithmic (lower) scale of the general formula derived from our proposed hypothesis (i.e., based on data of 1:3, 3:3, 6:3, black circles, general equation of $\tau = A\pi^{-n_{H_2O}}$ derived from equation 2 ($\tau \propto \pi^{-n_{H_2O}}$) where A is a constant determined by the fitting process, Figure 4, Figure S7, Figure S9, fitting method Ver. 1) and its application to the additional [Fe]:[catechol] ratio samples (i.e., 2:3, 4:3, blue-colored). The samples were dehydrated for 17.75 hours at 25 °C, 16 % R.H.. Given our observed trends (Figure 2), we know that the n_{H_2O} of 2:3 is between n_{H_2O} of 1:3 and 3:3; and n_{H_2O} of 4:3 is between 3:3 and 6:3. The τ of 2:3 and 4:3 were 725.35 s and 7780.91 s (blue diamonds), respectively, obtained from the step-strain test and Kohlrausch's stretched exponential fitting (equation 1). These values well abide by our model where the relaxation time of 2:3 are placed between the 1:3 and the 3:3 and that of 4:3 is between the 3:3 and the 6:3. Here, the n_{H_2O} of the 2:3 and 4:3 are estimated assuming the [Fe^{3+}] proportionally oxidizes the catechol to replace the normal catechol-Fe^{3+}-coordination[11] – i.e., 2:3 is in the midst of 1:3 and 3:3 while 4:3 is 1/3 apart from 3:3 and 2/3 apart from 6:3 in the x-axis. We note that the quantitative relation between the catechol oxidation and [Fe^{3+}] is not fully elucidated, especially in the high [Fe^{3+}] region, where the reaction may have reached the chemical equilibrium of maximum catechol oxidation.[11] Nonetheless, our observed relaxation times (blue diamonds) are very close to the coordinate output by our quantitative model (blue scissor marks on the red dotted trend lines).

References

(1) Jarzcki, A. A.; Anbar, A. D.; Spiro, T. G.; Jarzecki, A.; Anbar, A. D.; Spiro, T. G. DFT Analysis of Fe(H 2 O) 6 3+ and Fe(H 2 O) 6 2+ Structure and Vibrations; Implications for Isotope Fractionation. *J. Phys. Chem. A* **2004**, *108* (14), 2726–2732. https://doi.org/10.1021/JP036418B.

(2) Best, S. P.; Beattie, J. K.; Armstrong, R. S. Vibrational Spectroscopic Studies of Trivalent Hexa-Aqua-Cations: Single-Crystal Raman Spectra between 275 and 1 200 Cm^{-1} of the Caesium Alums of Titanium, Vanadium, Chromium, Iron, Gallium, and Indium. *Journal of the Chemical Society, Dalton Transactions* **1984**, No. 12, 2611–2624. https://doi.org/10.1039/DT9840002611.

(3) Schmitt, C. N. Z.; Winter, A.; Bertinetti, L.; Masic, A.; Strauch, P.; Harrington, M. J. Mechanical Homeostasis of a DOPA-Enriched Biological Coating from Mussels in Response to Metal Variation. *J R Soc Interface* **2015**, *12* (110), 20150466. https://doi.org/10.1098/rsif.2015.0466.

(4) Gottlieb, H. E.; Kotlyar, V.; Nudelman, A. NMR Chemical Shifts of Common Laboratory Solvents as Trace Impurities. *Journal of Organic Chemistry* **1997**, *62* (21), 7512–7515. https://doi.org/10.1021/jo971176v.

(5) Fulmer, G. R.; Miller, A. J. M.; Sherden, N. H.; Gottlieb, H. E.; Nudelman, A.; Stoltz, B. M.; Bercaw, J. E.; Goldberg, K. I. NMR Chemical Shifts of Trace Impurities: Common Laboratory Solvents, Organics, and Gases in Deuterated Solvents Relevant to the Organometallic Chemist. *Organometallics* **2010**, *29* (9), 2176–2179. https://doi.org/10.1021/om100106e.

(6) Lee, M.; Hong, M. Cryoprotection of Lipid Membranes for High-Resolution Solid-State NMR Studies of Membrane Peptides and Proteins at Low Temperature. *J Biomol NMR* **2014**, *59* (4), 263–277. https://doi.org/10.1007/s10858-014-9845-z.

(7) White, P. B.; Wang, T.; Park, Y. B.; Cosgrove, D. J.; Hong, M. Water–Polysaccharide Interactions in the Primary Cell Wall of *Arabidopsis Thaliana* from Polarization Transfer Solid-State NMR. *J Am Chem Soc* **2014**, *136* (29), 10399–10409. https://doi.org/10.1021/ja504108h.

(8) Dust, J. M.; Fang, Z.-H.; Harris, J. M. Proton NMR Characterization of Poly(Ethy1ene Glycols) and Derivatives. *Macromolecules* **1990**, *23*, 3742–3746. https://doi.org/10.1021/ma00218a005.

(9) Kim, S.; Peterson, A. M.; Holten-Andersen, N. Enhanced Water Retention Maintains Energy Dissipation in Dehydrated Metal-Coordinate Polymer Networks: Another Role for Fe-Catechol Cross-Links? *Chemistry of Materials* **2018**, *30* (11), 3648–3655. https://doi.org/10.1021/acs.chemmater.7b05246.

(10) Kim, C.; Ejima, H.; Yoshie, N. Non-Swellable Self-Healing Polymer with Long-Term Stability under Seawater. *RSC Adv.* **2017**, *7* (31), 19288–19295. https://doi.org/10.1039/C7RA01778B.

(11) Fullenkamp, D. E.; Barrett, D. G.; Miller, D. R.; Kurutz, J. W.; Messersmith, P. B. PH-Dependent Cross-Linking of Catechols through Oxidation via Fe(3+) and Potential Implications for Mussel Adhesion. *RSC Adv* **2014**, *4* (48), 25127–25134. https://doi.org/10.1039/c4ra03178d.